

Solar grade silicon production: A review of kinetic, thermodynamic and fluid dynamics based continuum scale modeling



Shwetank Yadav^a, Kinnor Chattopadhyay^a, Chandra Veer Singh^{a,b,*}

^a Department of Materials Science and Engineering, University of Toronto, Canada

^b Department of Mechanical and Industrial Engineering, University of Toronto, Canada

A B S T R A C T

The rapid growth in silicon photovoltaics deployment has led to increased research focus on the energy and capital intensive refining of solar grade silicon for improved environmental, production and economic benefits. As this process consists of a number of steps taking place in multi-phase reacting systems with complex fluid and energy flows, models can be an important tool for mechanistic understanding, design and optimization. This paper reviews models for the most widely implemented refining techniques and classifies them into two broad categories; those relating to the synthesis of volatile Si based compounds and those relating to the deposition of volatile silicon based compounds. Within each category, models are further divided according to the reactor type or physical process which they are examining. These models typically use computational techniques with various combinations of theory for obtaining chemical thermodynamics, chemical kinetics, fluid mechanics and heat and mass transfer information for a system. The system definition, main assumptions, computational techniques and main results for each study are presented. There is also a brief review of ab initio atomistic studies for this area along with a discussion for future research. This work should help researchers in selecting appropriate physical and chemical models for investigating solar grade silicon refining or further developing their own models.

1. Introduction

Solar photovoltaics (PV) are increasingly moving into mainstream energy generation and have experienced explosive growth over the past decade [1]. Cumulative global installed solar PV capacity has grown from just 2 GW in 2004 to 178 GW in 2014 and is predicted to increase in an exponential fashion to hit almost 700 GW in 2020 [2]. This has been accompanied by a decrease in the price of PV systems by around 75% in less than ten years [3]. Worldwide PV module manufacturing capacity is expected to hit 95.4 GW in 2016 and the annual PV market is expected to hit 135 GW by 2020 [4]. This tremendous past and expected future growth has led to increased focus on improving the PV manufacturing process in terms of cost and output [5].

Silicon based modules dominate the PV industry, with silicon wafer technology accounting for 92% of world production in 2014 [6]. The majority of these are made using polysilicon and the silicon wafers account for half the cost of the PV module [7,8]. Polysilicon has undergone drastic market price swings over the last decade and a half, caused by supply-demand imbalances as well manufacturing cost

differences [9]. As polysilicon serves as the feedstock for PV manufacturing technologies, significantly impacting all downstream components of the PV supply chain and their costs, the production of solar grade polysilicon (SOG-Si) is of particular interest.

The overall silicon PV production process is shown in Fig. 1. Metallurgical grade silicon (MG-Si) of about 98.5% purity is produced by the carbothermic reduction of silicates in electric arc furnaces [10]. This MG-Si is then refined to produce SOG-Si (which has a minimum of 6N or 99.9999% purity) polysilicon (also known as poly-crystalline silicon). This step is generally accomplished via chemical conversion of MG-Si to gaseous Si based compounds and vapor deposition of these into solid silicon rods. The silicon rods are subsequently melted, recrystallized and then cut to produce either monocrystalline or multicrystalline silicon wafers depending on the process used. Silicon wafers are chemically treated, doped, coated and provided with electrical contacts to produced solar cells. These solar cells are then finally assembled into panels which integrate micro-electronics, mounting frames and other components in various configurations dictated by downstream companies to make solar modules.

The step involving production of SOG-Si from MG-Si, currently

* Corresponding author at: 184 College St., Suite 140, Toronto, Ontario, Canada M5S 3E4.
E-mail address: chandraseer.singh@utoronto.ca (C.V. Singh).

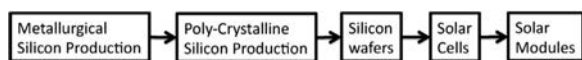


Fig. 1. Silicon PV module manufacturing process [10].

consists of very energy and capital intensive process with limited throughput. Hence, process and technology improvements for this step will have significant benefits for PV panel production and are a major area of research. Mathematical models can provide mechanistic insights for optimizing operating conditions or enabling new designs which can overcome some of these challenges. Therefore, they form an important tool for improving SOG-Si production processes and can contribute towards eventually increasing output and decreasing costs of Si PV panels.

This work specifically reviews numerical models incorporating thermodynamics, reaction kinetics, fluid dynamics and heat and mass transfer calculations for investigating MG-Si to SOG-Si production. As such, it will help researchers in selecting appropriate models for studying a particular experimental setup, optimizing a process or creating new designs while also identifying opportunities for future research. An overview of methods for producing polysilicon is first presented. Then in-depth reviews of the literature are presented for each of the two major sub-steps of MG-Si to SOG-Si production; namely the conversion of MG-Si to Si based compounds and SOG-Si production from these compounds. This is followed by a brief discussion of atomistic scale models (which are not explored in detail in this review) and future challenges and areas for improvement.

2. Synopsis of the current MG-Si to SOG-Si production technologies

The typical method for producing SOG-Si involves conversion MG-Si to intermediate Si based compounds, purification of these intermediate species and then reduction or thermal decomposition of these species into high purity silicon. Fig. 2 provides an overview of conventional processes and those under development. The most

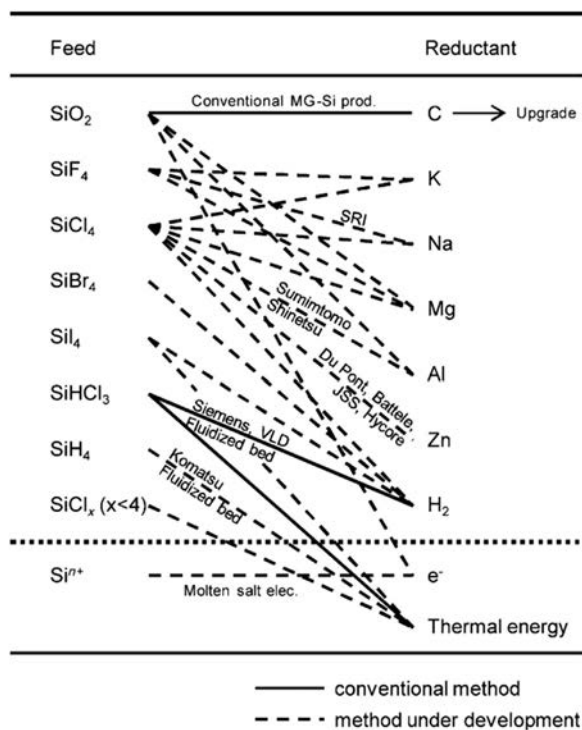


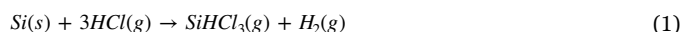
Fig. 2. Refining pathways for producing solar grade silicon using intermediate Si based compounds (feed) and their subsequent reduction/decomposition through agents (reductant) [12].

important of these is the Siemens process, which accounts for approximately 90% of worldwide polysilicon production [11].

2.1. Siemens process and derivations

This process chiefly relies on the intermediate of trichlorosilane (SiHCl_3), commonly abbreviated as TCS. Fig. 3 provides a detailed overview of the Siemens process. The basic method can be broken down into four major parts: the production of TCS from MG-Si, the purification of TCS, the reduction or thermal decomposition of TCS into solid polysilicon and the recycling of byproducts and recovery of remaining TCS.

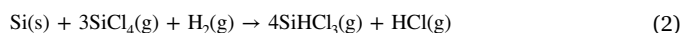
The initial step involves hydrochlorination of crushed MG-Si in a fluidized bed reactor to produce TCS at temperatures ranging from 573 to 623 K [12,13] through the following reaction:



Although there are a number of possible side reactions, 90% of the yield is TCS with the major other product being silicon tetrachloride (SiCl_4 or STC). The TCS gas is then purified through distillation, often passing through multiple distillation columns, which removes most of the STC. The resulting purified TCS is then fed into a bell shaped reactor containing seed silicon rods which are heated through electrical resistance to between 1273 K and 1373 K. TCS will start decomposition to form Si above 675 K and deposit onto the Si rods. However, the exact mechanism by which this occurs is complex and the reactions occurring are presented in varied forms in the literature.

Overall, TCS is either thermally decomposed or reduced by H_2 (with both possibly occurring simultaneously [14–16]) to eventually produce Si as well as HCl, STC, SiCl_2 , SiH_2Cl_2 (dichlorosilane or DCS) and H_2 through a series of reactions. The overall reaction system is complex and there is not an agreement in the literature as to the exact mechanisms and elementary steps. The SiCl_2 is thought to play a pivotal role as an intermediate species through surface adsorption on Si rods. The exact set of equilibrium reactions, as well as other chemical compounds likely present, are discussed in more detail in Section 3.1. The Si rods increase in diameter to a set size after which they are removed from the reactor. The slow deposition rate and batch nature of the procedure and the fact that most of the energy input to the reactor is not used in actual silicon production, due to thermal and other losses, results in an energetically inefficient and slow output process [17].

The remaining gases from the bell jar reactor, containing the compounds listed in the previous paragraph, are then recovered and separated through distillation. The H_2 and TCS are fed back into the bell reactor and the HCl is fed into the MG-Si hydrochlorination reactor. The STC has to be disposed and may be used for producing SiO_2 which is then subsequently used to make MG-Si. However, as three to four moles of STC are produced for every mole of polysilicon produced, there has been the development of a modified Siemens process in which STC is combined with H_2 and MG-Si to produce TCS during the hydrochlorination step [18], acting as the chlorine source instead of HCl, with the following overall reaction:



This modified Siemens process hence finds a use for the STC product and eliminates the need to add fresh HCl to the cycle; however, it requires the hydrochlorination to take place at higher temperatures of 773–873 K. Neither approach has a clear economic advantage which would apply to every manufacturing environment and both the original and modified Siemens processes are widely used in industry [11]. This recycling of STC to produce TCS can also be achieved through plasma and non-MG-Si based catalytic hydrogenation processes, however these both have serious issues (high energy usage for the former and very low TCS yield for the latter) and are not used significantly in industrial production.

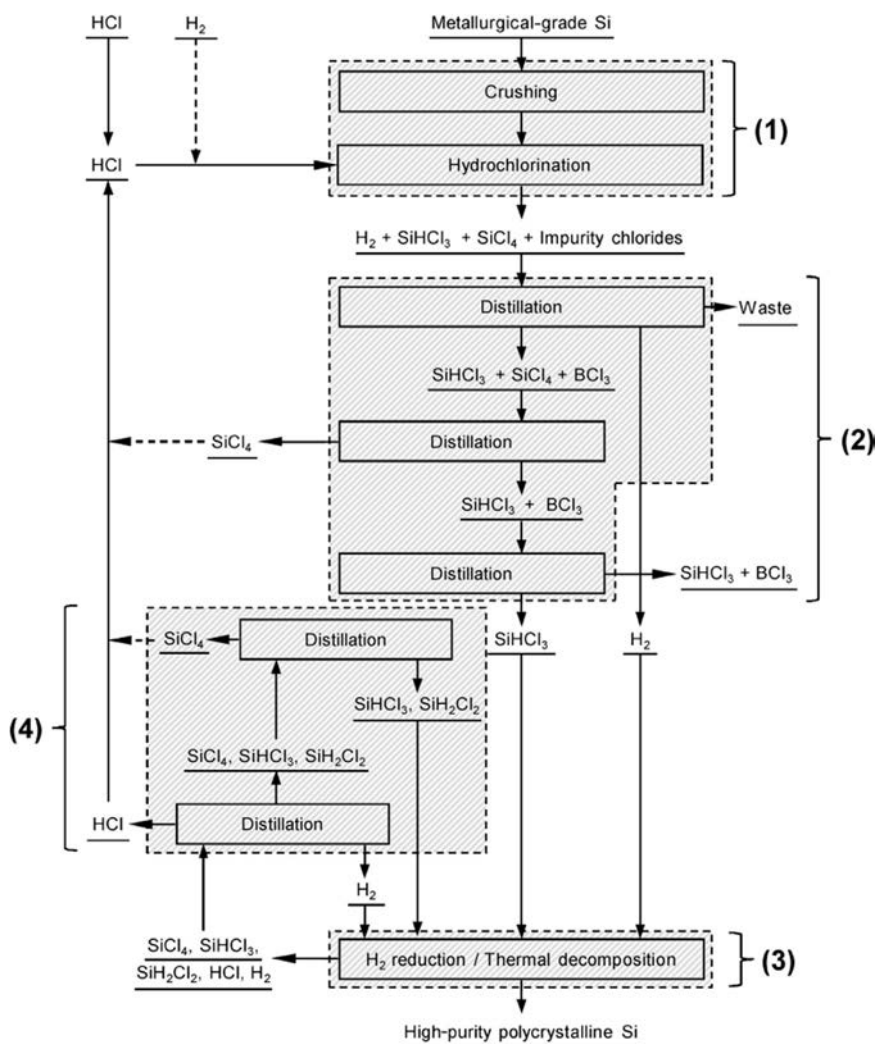


Fig. 3. Detailed process flowchart of the Siemens process [12]. (1) Production of TCS from MG-Si (2) Purification of TCS (3) Reduction/deposition of TCS into SOG-Si (4) Recovery and recycle of byproducts.

2.2. Silane pyrolysis

The second most widely used commercial process, accounting for almost all of the non-Siemens technology based production, utilizes the decomposition of silane (SiH_4). The Komatsu/Union Carbide (UCC) process [19] is a development of the Siemens process in which silane is produced subsequent to the hydrochlorination and distillation steps by disproportionation of TCS and DCS through catalytic redistribution. Other methods for producing silane involve hydrogenation of SiF_4 by metal hydrides (ethyl corporation/MEMC method) or reacting silicon and magnesium powders in the presence of ammonia and hydrogen chloride. The resulting gases (which include STC as a byproduct) are further distilled to isolate silane. The silane is then thermally decomposed according to the following overall (pyrolysis) reaction



It should be noted that, as with TCS decomposition, pyrolysis can have a complex set of elementary steps and side-reactions and there is no agreement on the exact mechanisms in the literature. Generally, silane pyrolysis is broadly divided into two types of reactions: heterogeneous and homogeneous decomposition. Heterogeneous decomposition takes place on the silicon substrate and is the dominant and more desirable route. Homogeneous decomposition takes place away from the surface and results in formation of gaseous silicon which is often referred to as fines and viewed as undesirable. These can be scavenged

and become part of larger particles and eventually deposit on to silicon substrate or end up leading the reactor as dust and cause fouling and unwanted deposition issues.

In the Komatsu/UCC process, the decomposition is done in a bell jar reactor at 1073 K in a similar manner to the Siemens process. This lower temperature results in energy savings compared to the Siemens process, however the production of silane itself involves more steps and higher cost as well as more difficulty in handling of the gas.

The low deposition rate, high energy consumption and batch nature of bell jar reactor operation have led to the development of fluidized bed reactors (FBR) for the decomposition step in both Siemens and silane processes. Filtvedt et al. [20], give an excellent review of the history of FBR development for silicon production as well as a summary of earlier (prior to the mid-2000 s) numerical modeling efforts for these systems. In these reactors, seed Si particles are injected from the top of the reactor while the reactant gases (TCS or silane based) are blown upwards from the bottom of the reactor and carry the particles with them. The previous decomposition/reduction reactions for the bell reactor now take place on the surface of these particles instead of Si rods and the particles grow until they are of a specific size (and weight) and fall out of the reactor. This setup provides a much higher surface area for the Si deposition reactions and allows for continuous operation, thereby greatly increasing Si production rates. Furthermore, FBRs also have lower energy requirements without the large losses incurred by resistive heating. However, challenges related

to fines control, deposition on reactor walls and contamination remain [11,13]. Li et al. [21] reviewed these technical challenges and relevant research literature on them, particularly studies on elucidating fines formation mechanisms (with most studies finding it is a complex gas-solid chemical system dominated by silicon hydrides) and attempting to heat the FBR while avoiding deposition on the walls and heating source (with external heating, recirculating or sectioned designs being proposed).

Filtvedt et al. [22] further addressed FBR modeling and scale-up by reviewing silane deposition mechanisms, microscale effects and how they have been incorporated into reactor models. They classified reactor models as belonging to two major types. The first type of model were two phase phenomenological based models utilizing analytical relationships which divide the bed into distinct bubble (mostly gas voids) and emulsion (containing seed particles) phase regions, with occasional consideration of a cloud phase between these two, and their variants. The second type of models utilized detailed computational fluid dynamics (CFD) further divided into Euler-Euler models (the two gas and solid phases are treated as an interpenetrating continuum where momentum equations are solved for both at the same time) or discrete element method type models where the gas is treated as continuum but individual particles are modeled with Newtonian motion. Filtvedt et al. also discussed the modeling and scale-up of spouted bed reactors.

2.3. Alternative Processes

There are a limited set of numerical modeling studies on non-Siemens (TCS or silane decomposition by heat) derived processes. Hou et al. [23] have done a preliminary thermodynamic study of SiCl₂ behavior during Zn reduction of STC. Furthermore, as a substitute for the processes involving intermediate Si based compounds highlighted above, MG-Si can be directly refined (or upgraded) through metallurgical methods. Acid leaching of crushed MG-Si is able to remove some impurities but is still under study [12]. Directional solidification is able to remove a great deal of impurities [24] but must be followed by further refining such as slag treatment to remove remaining phosphorous and boron. Karabanov et al. gave a brief overview of chlorine-free processes involving solid extraction and modeling basics [25]. Additional methods of direct upgrading of MG-Si under development involve plasma chemical refining (with numerical modeling by Karabanov et al. [26]), vaporization of impurities under oxidizing conditions by electron beam or irradiation and vacuum refining [27]. The direct electrolytic reduction of SiO₂ (which is used to make MG-Si) to SOG-Si has also been considered [28]. However, none of these methods has achieved commercial deployment of significance and will not be considered further in this paper.

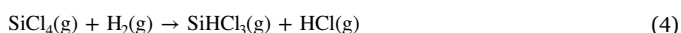
3. Synthesis of Si Based compounds from MG-Si

3.1. Hydrochlorination of Si

The various studies on silicon hydrochlorination are summarized in Table 1 along with details of their models and main representative equations.

3.1.1. Fixed bed reactors

Sugiura et al. looked at the hydrogenation of STC in a fixed bed reactor at temperatures from 1023 K to 1123 K [29]. They considered it in two forms, first as a gas phase only reaction:



Second as a two-step gas-solid reaction with sequential reactions involving first the gas phase in (4) and then the gas-solid reaction in (1). The gas phase only reaction was assumed to follow second order reversible rate equations while the second reaction of the gas-solid

reaction involving Si (and using HCl produced from the gas phase only reaction) was assumed to follow a first order rate equation incorporating gas void fraction, silicon particle radius and shape factor. The resulting expression is shown in Table 1. A segment compartment model for 1-D plug flow was used for reactor performance and rate constant determination, dividing the fixed bed column into 100 segments with mass balances performed for each compound around each segment.

Under the assumptions that the reactions are steady state, that convective mass transfer terms dominate over diffusion transport thus allowing elimination of the diffusion terms and an isothermal temperature throughout the reactor; the partial differential mass balance equations were reduced to ordinary differential equations solved using simple finite difference method. Using reactor inlet conditions as one set of boundary conditions, a best fit trial and error method which matched calculated outlet molar ratios with experimental values was used to find the rate constants. Higher conversions were found for higher temperatures and longer residence times as well by using larger input ratios of STC to H₂. There was generally good agreement between model calculations and experiment, although the gas phase only reaction matched calculations better than the gas-solid reaction. For the latter case, the authors speculate that 1-D plug flow model and first order kinetics might not be sufficient to capture the complexity of the reacting system.

A mathematical model for chlorination of Si particles using Cl₂ gas to produce STC was developed by Seo et al. [30]. First, they developed a kinetic expression for the reaction between chlorine and a single Si particle under the following assumptions:



- the chlorination reaction is irreversible
- the reaction is first order with respect to chlorine
- gases are ideal
- the silicon particle is spherical
- kinetics are described by the unreacted core model for particles decreasing in size with time
- there is no ash layer formation.

This model assumes that the reaction is controlled by mass transfer to the surface of the sphere and chemical reaction occurring in series. The mass transfer coefficient was expressed using a correlation proposed by Kato et al. [31] for gas-solid mass transfer in fixed beds at low Reynolds numbers. An expression relating the radius of the Si particle to chlorine concentration and molar density was derived.

An expression (see Table 1) for a bed containing *N* Si particles was then obtained by doing a mass balance of chlorine gas around a control volume (CV) inside the bed with the following assumptions: only the axial direction of the bed is considered for convective transport, the bed is considered isothermic at atmospheric pressure, particles do not move in the bed, bed inlet gas is entirely pure chlorine, the total rate constant does not vary axially and the whole bed is exposed to an average concentration of chlorine, diffusive transport is neglected, there is no accumulation in gas phase due to quasi-steady state conditions. A computer code which calculates instantaneous and average mass transfer coefficients, chemical reaction and mass transfer resistances and silicon conversions was used. Reaction rate constants were obtained by fitting with experimental data. This model was for a non-compacted bed; compacted beds (in which the diffusion term cannot be neglected) were modeled by treating the mass transfer coefficient as a fitting parameter evaluated from compacted bed experimental data.

The mass transfer coefficient *k_g* was found to almost stay constant with temperature (753–953 K) while reaction rate constant *k_r* increased with temperature, displaying the greater sensitivity of the latter. The *k_g* value decreased with increased compaction (affecting

Table 1

Theoretical studies of silicon hydrochlorination. FxB is fixed bed reactor, FuB is fluidized bed reactor, SS is steady state, IsoT is isothermal, rxn means reaction, R is reaction rate, T is temperature, C is concentration, r is radius of particles, m is mass, M is molar weight, 0 subscript represents initial value, ρ is density, t is time, p_i is partial pressure, P is total pressure, K_f fluidized bed reaction rate constant, K_r fixed bed reaction rate constant, K_{bc} , vol. rate of gas exchange between bubble, K_{ex} vol. rate of gas exchange between cloud-wake and emulsion phase, Y_b ratio of solids vol. in bubble phase to bubble vol. in bed, Y_c ratio of solids vol. in cloud-wake region to bubble vol. in bed, Y_e ratio of solids vol. in emulsion phase to bubble vol. in bed.

Study	Model System	Model Assumptions	Factors Considered	Representative equation	Equation Notes
Sugiura et al. [29]	FxB, 1-D plug flow, segmented compartments	SS, idea gases, IsoT, Neglect diffusive MT	gas void fraction, particle radius, shape factor	$R_{Si} = \phi(1 - \epsilon)/X_0 k_{HCl}$	k rate constant for reaction (1), ϕ shape factor Si particle, ϵ gas void fraction, X_0 avg. Si particle radius, k rate constant reaction (4)
Seo et al. [30]	FxB, 1-D	quasi-SS, ideal gases, IsoT, reaction controlled by mass transfer to surface, diffusive transport ignored	shrinking core, bed compaction, bed height	$r_0 - r = \frac{1}{2} \frac{C_{p,0} \mu_0^2 M_{Si}}{3m_0^2} \left[1 - \exp\left(-\frac{-3m_0^2 r_0^2}{4\mu_0^2 \phi_{Si}}\right) \right]$	For compact beds; r Si particle radius, u gas velocity, A bed cross-section area, k rate constant reaction (5),
Noda et al. [33]	FuB, 1-D	equal sized Si spheres, isotropic rxn at constant rate, new surfaces created by rxn become active & spread	shrinking core with surface roughness, Langmuir adsorption	$R_{TCS} = \frac{\rho_{Si} R_{Si}}{M_{Si}} \frac{S_0}{S_0} = f \left[1 - \exp\left(-\frac{\pi N k_c^2 r^2}{S_0}\right) \right] (1 - c_r)^{2/3}$	S_0 activated surface area of Si/unit vol. reactor, S_c area of activated surface of Si particles, S_0 initial surface area, N no. active points on Si particle, $R_{Si} = k_0 \rho_{Si}^{0.5}$ from expt., c_r conversion ratio of Si particles
Jain et al. [34]	FuB, 1-D, compartmental (for Kato-Wen model), Kunii-Levenspiel (K-L)	IsoT, gas completely mixed in each phase, bubble phase has spherical bubbles surrounded by spherical clouds	3 phases: bubble, emulsion & cloud; particle size, fluidization velocity, freeboard region	$K_f = C_f K_r + 1/(1/K_{bc} + (1/r_c K_r + 1/(1/K_{cr} + 1/r_c K_r)))$ $(1 - X_A) = \exp(-K_f L_f/U_b)$	Kunii-Levenspiel (K-L) model, X_A HCl conversion, U_b bubble velocity, L_f bed height, see caption for other terms
Wang [35]	FuB, 2-D, gas-solid plug flow, cylindrical reactor with coolant tube in center	uniform distribution of particles (but not uniform size), constant $c_{p,cool}$ constant coolant T, insulated wall	shrinking core; heat generated by reaction, heat transfer to coolant & particle motion	$R_{Si} = - \left[\frac{1}{3} k_1 + \frac{1}{4} k_2 \right] C_{HCl} \mu_{p,Si} \frac{\partial T}{\partial x} - h \left(\frac{\partial^2 T}{\partial x^2} + \frac{1}{x} \frac{\partial T}{\partial x} \right) - h \left(\frac{\partial^2 T}{\partial x^2} \right) + \dot{g} = \rho C_p \frac{\partial T}{\partial t}$	k_1 & k_2 are 1st order rate constants for reactions (6) and (7), u is velocity of gas/solid stream, h is effective heat transfer between coolant and FuB, \dot{g} is reaction heat generation
Ding et al. [32]	FxB, Cu-Si catalytic surface rxn	Langmuir-Hinshelwood(L-H) or Eley-Rideal(E-L) catalysis, initial c_{TCS} zero	five reaction schemes based on different elementary step combinations, surface site regeneration	$-R_{Si} = \frac{\frac{K_1 K_2}{K_3} P_{TCS}^2 H_2 \left(1 - \frac{P_{TCS}^2}{K_4 P_{Si}^2 H_2} \right)}{1 + K_1 P_{TCS} + \frac{K_2}{K_3} P_{TCS}^2}$	Based on E-L mechanism which best represents experiment, K_i elementary step equilibrium constant, K_3 equilibrium constant for entire system in terms of P_i
Ding et al. [36]	Thermodynamic equilibrium	ideal gases, ignore Si vol. change with P	3 reactions with 6 chemical species, gas phase fugacities, varying T, P, initial molar ratios,	$G_T = \sum_{i=1}^{N-1} n_i \left(G_i^\circ + RT \ln \frac{p_i}{P^\circ} \right) + n_{Si} G_{Si}^\circ + n_{Si} V_{Si} (P - P^\circ)$	G_T total Gibbs free energy, h_i gas phase molar fraction, V_{Si} Si molar volume
Wu et al. [37]	Thermodynamic equilibrium	low temperature hydrogenation $SiCl_4$ -Si- H_2 system	7 reactions with 7 chemical species, varying T, P, initial molar ratios	$\Delta G_T^\circ = \left(\Delta H_{298}^\circ + \int_{298}^T \Delta C_p dT \right) - T \left(\Delta S_{298}^\circ + \int_{298}^T \frac{\Delta C_p dT}{T} \right)$ where $\Delta C_p = \Delta a + \Delta bT + \Delta cT^2 + \Delta dT^3 + \Delta eT^4$	G_T total Gibbs free energy, H enthalpy, S entropy,
Kumioishi et al. [38]	1-D plug flow with high T hydrogenation and cooling section	SS, IsoT, ideal flow, IsoB,	63 reactions with 26 chemical species, T, cooling rate, initial molar ratio	$\rho_w \frac{dX_k}{dx} = W_k \phi_k$	v is flow velocity, W_k is molar weight and ϕ_k is molar production rate of species k
Colomb et al. [39]	FuB, Fe catalyzed, optional Cu catalyst, modified K-L	IsoT, Fe naturally present in MG-Si, HCl addition effect through doubling active Fe, ignore separate cloud phase	non-linear bubble growth in industrial reactors, particle size distribution beyond K-L model limits	$-\frac{dC_{ib}}{dz} = f_{p,Si} \nu_{Fe} R_{Fe,Si} + \gamma_{Cu} R_{Cu,Si} + \delta K_{bc} (C_{ib} - C_{e,r})$ $\delta K_{bc} (C_{ib} - C_{e,r}) \cong f_{p,Si} \nu_{Fe} R_{Fe,Si} + \gamma_{Cu} R_{Cu,Si} + \gamma_{Cu} R_{Cu,Si}^k$	i component (STC, TCS, H_2), u superficial velocity, z reactor height, f vol. solid/vol. bed, b subscript bubble phase, e subscript emulsion phase, γ fractional catalyst weight

porosity) while k_r stayed the same. Decreasing bed height also increased k_g , however compacting had greater influence on the coefficient values.

Ding et al. [32] looked at hydrochlorination in the presence of CuCl_2 catalyst. Looking at previous studies and their own experimental data, they proposed a general reaction network which involved adsorption of reactant onto Cu-Si surface species, surface reaction between STC and H_2 to produce TCS and adsorbed HCl, desorption of TCS to bulk gas, surface reaction between adsorbed HCl and occupied Cu-Si site to form TCS and H_2 and breakage of Cu-Si bonds, desorption of TCS and H_2 to bulk gas and the regeneration of Cu-Si active sites through copper diffusion to combine with free silicon atoms. The Langmuir-Hinshelwood (L-H) and Eley-Rideal (E-H) models were tested to model the system and compare with experiment. After deriving reaction rate expressions for each elementary step (all assumed to follow first order kinetics) model discrimination was applied to both models. This was based on initial rate trends, with TCS concentration assumed zero, so that rate equations would simplify to expressions of STC and H_2 concentrations. Experiments with these conditions were then conducted and, after comparison, the E-R model consisting of three elementary steps was found to best describe the system. Kinetic parameters were subsequently derived from experiments. The resulting model matched experimental results for STC conversion very well, as can be seen in Fig. 4. The model suggested that the surface reaction between adsorbed STC and gas-phase H_2 was the rate determining step.

3.1.2. Fluidized bed reactors

Noda et al. [33] investigated the reaction of HCl with Si particles to produce chlorosilanes in a fluidized bed reactor at temperatures of

623–723 K. They used a model based on the shrinking core model, but taking into account both shrinking Si particle size and its changing surface roughness; in this the surface reaction only occurs at active points which are breaks in native oxide layers. It was assumed that Si were spheres of the same size with initially N such active sites, that the reaction proceeds isotropically at a constant rate and that new surfaces created by the reaction become active surfaces and spread. After multiple active surfaces meet and overlap, the entire surface becomes active. Although the model matched accompanying experimental results reasonably well in most cases, excepting cases where the HCl conversion ratio approached 1, the authors cited impurities as the problem for those few cases where model and experiment did not line up. The authors concluded that the reaction followed 0.5 order kinetics in terms of HCl concentration while the production of STC (along with other unstable chlorosilanes) could be ignored because it was more than hundredfold lower. Under Langmuir type reaction scheme, the adsorption of HCl on Si sites could not be the rate-determining step. However, it was not possible to determine whether desorption of TCS or H_2 would be the rate determining step. Ultimately, an expression for overall TCS production per reactor volume in terms of Si density, activated Si surface area and HCl concentration was derived for HCl concentrations in the range 0.15–1.8 mol/m³.

Hydrochlorination of Si in a fluidized bed reactor was also examined by Jain et al. [34] at atmospheric pressure, 589–599 K and average Si particle size from 88 to 208 μm . The authors tested the Kunii and Levenspiel (K-L) [40] and Kato and Wen (K-W) [41] models for gas-solid fluidized beds; both models are based on three-phase theory involving bubble, emulsion and cloud phases. The K-L model predicts HCl conversion based conditions in the fluidized bed; including gas velocity, bubble velocity and reaction rate constants. The K-W model

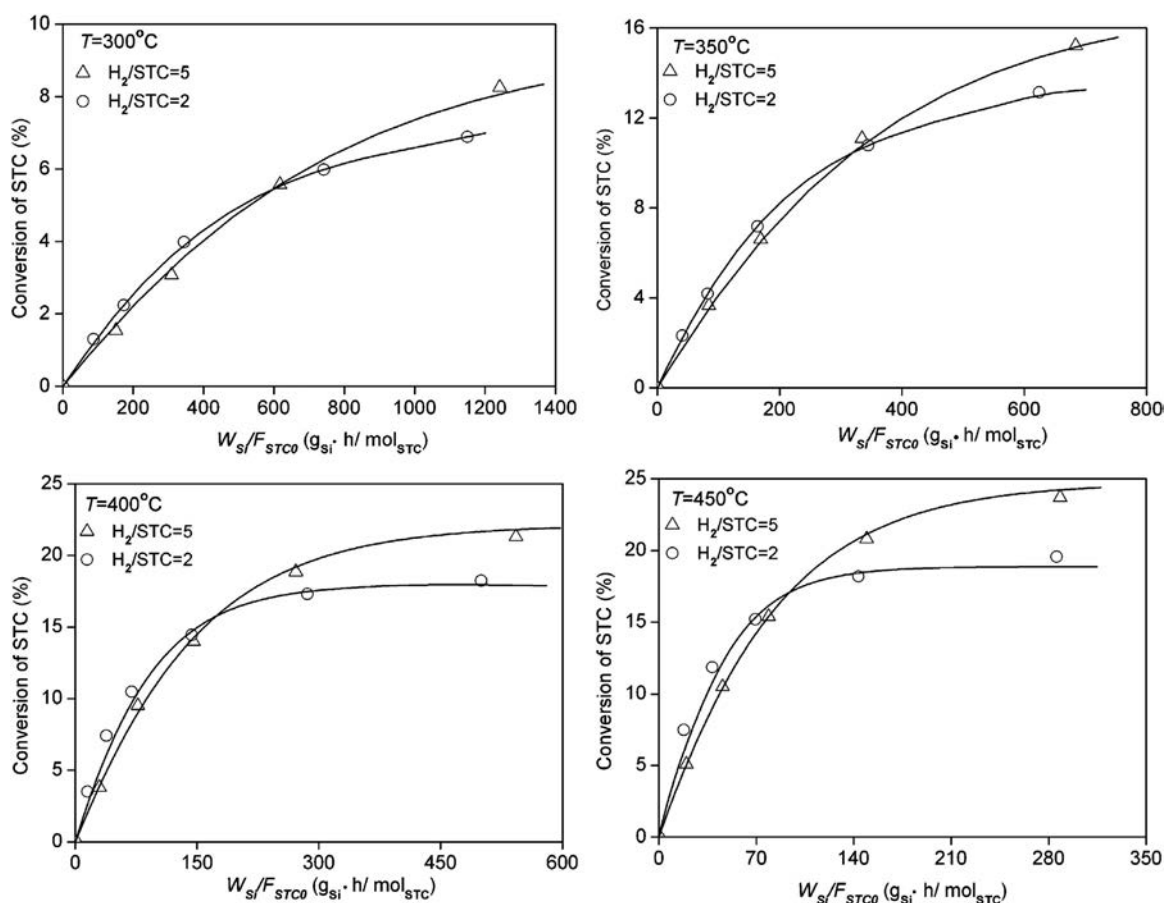


Fig. 4. Comparison of calculated and experimental STC conversion for CuCl_2 catalyzed hydrochlorination at four different temperatures in Ding et al.'s [32] work. W_s is initial silicon weight (in g_s) and F_{STC0} is initial STC molar flow rate. Reprinted with permission from [32]. Copyright 2014, American Chemical Society.

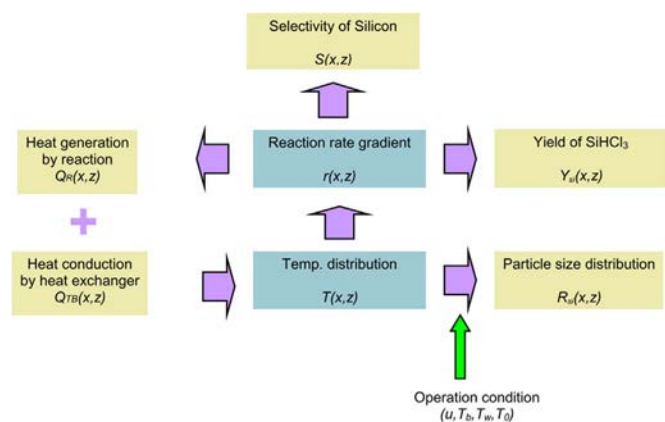
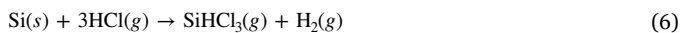


Fig. 5. Energy balance model and influencing factors for 2D model of fluidized bed reactor for MG-Si hydrochlorination used by Wang [35].

(also known as bubble assemblage model) is a compartmental model which gives the HCl concentration in each compartment. A further modification of the K-L method, which takes into account the freeboard region [42] (region from above the bubbling bed to the exit point) was also applied. A fixed bed rate constant, needed for expressions in the model, was obtained from experimental data. Fluidization velocities were calculated using Chisetar et al.'s [43] expression for particles above 100μ and Wen and Yu's [44] equation for fine particles below 100μ . All three models predicted an overall trend in which smaller particle diameter produced greater HCl conversion, although none exhibited a monotonic pattern. This trend was obeyed monotonically by experimental data, with all the models under predicting HCl conversion and the K-W model coming closest to experiment. The authors concluded that the models they tested were not satisfactory and a more suitable model needs to be developed for this system.

Wang [35] examined the non-catalytic hydrochlorination of MG-Si in an FBR using a 2-D temperature model along with kinetic expressions to obtain temperature distribution in the reactor and the effect of varying operating conditions. An overview of the modeling scheme is presented in Fig. 5. The author attempted to take into consideration particle structure change with time and temperature, selecting to use a non-porous shrinking core model for solid undergoing gasification which assumes reaction occurs at a sharp interface between the exhausted outer shell and unreacted core of the solid. No product layer exists and hence there is no ash diffusion resistance. For heat transfer, a radial as well as transverse temperature distribution was assumed along a cylinder shaped reactor with a coolant tube in the center. Heat transfer between reactor walls and reactor fluids was also taken into account. A constant gas phase concentration was assumed and gas-solid flow was assumed to occur as plug-flow.

Furthermore, it was assumed there was a uniform distribution of solid particles resulting in a constant number of silicon particles in each unit volume. Although particle sizes decrease with reaction, they were not considered to be completely consumed. Reaction rates were expressed as being proportional to available unreacted surface area, taking place across the entire surface of the spherical particle. Only the kinetics of two gas-solid surface reactions were considered in the study, one producing TCS (6) and the other producing STC (7), with both following first order rate kinetics with regards to HCl concentration (these kinetic coefficients were obtained from previous literature) and exhibiting exothermic behavior.



The heat generated by reaction, heat transfer between coolant tube and fluidized bed and heat transfer caused by particle motion were included for the energy balance calculations of the system. Partial differential

expressions for energy were derived based on a differential volume in the shape of a pipe segment (with dimensions Δx in radial direction and Δz along axial length of reactor). Mass balance equations were similarly calculated, but were further simplified under steady state assumption for chemical species concentration as previously stated. After integration, this allowed for the expression of particle radius distribution in the axial z -direction in terms of the velocity of the solid flux.

The energy partial differential equations were solved using finite difference methods through the Crank-Nicolson method. This divides the cross-section equally into unit parts called differential operators and was used with central finite differences method. The heat dispersion in the z -direction was neglected as temperature gradient was dominated by particle movement in this direction. The expressions were further simplified under steady state conditions. Boundary conditions consisted of central coolant temperature (considered constant with negligible gradient) and a reactor wall which was considered to be insulated. Equations were then numerically solved using MATLAB.

The calculated temperature distribution indicated that overall temperatures increased from reactor center to wall (in positive x -direction) and from reactor entrance to exit (along positive z -direction) as seen in Fig. 6. The reaction rate was also found to be higher at the center than closer to the wall, indicating higher temperature may reduce TCS production. Si particle radius decreased along z and x . The velocity of the feed stream was found to have little impact on temperature and reaction rate distribution. The overall yield of TCS (summed over all points) was thus found to be 36.8% at 523 K initial feed temperature. Changing the initial temperature did have an influence on both temperature and reaction rate distribution, lowering yield with increasing temperature down to 10.6% at 623 K. The temperature of the coolant tube was also found to influence temperature distribution and reaction rates, with lower coolant temperatures increasing TCS yield and producing 48.5% yield at 453 K. The effects of varying thermal conductivity between coolant tube and fluidized bed and heat capacity of the fluid were found to be negligible. The reactor size had only slight impacts on temperature and reaction rates, with increasing diameter and length slightly increasing TCS yield (a 3.5 by 4.5 m reactor produced a best of 36.9% yield). In terms of sensitivity analysis, the parameters affecting results the most are the reaction rate constants, with the second constant for production of STC having greatest impact. The author concluded that there should be more up to date investigations of these fundamental constant values to increase the robustness of the model.

Colomb et al. [39] looked at production of electronic grade silicon through silicon hydrochlorination, however the reacting system is exactly the same and can be applied for SOG-Si production. They attempted to recreate the experimental results of bench scale FBRs in literature which tested the addition of HCl and copper catalyst as an extension of normal STC and hydrogen based hydrochlorination. Reaction kinetics were modeled based on the mechanisms of Becker [45] who suggested that hydrochlorination took place through an iron catalyzed reaction (using iron naturally found in MG-Si) in parallel with a copper catalyzed reaction when the latter was present. Kinetic rate laws based on power laws were chosen as they produced the least deviation from experimental results, indicating the reactions were based on chemisorption of reactant species.

A modification of the K-L model was derived from first principles wherein the cloud phase was assumed to be very thin and have the same chemical concentration as emulsion phase. The modified model is also valid for Geldart AB group [46] and particles that have just transitioned into Geldart B, as opposed to being valid for just Geldart A and AB particles. A bubble size prediction correlation based on Yasui and Johanson's work [47] was also used to capture the non-linear behavior in growth of bubbles along bed height found in industrial reactors.

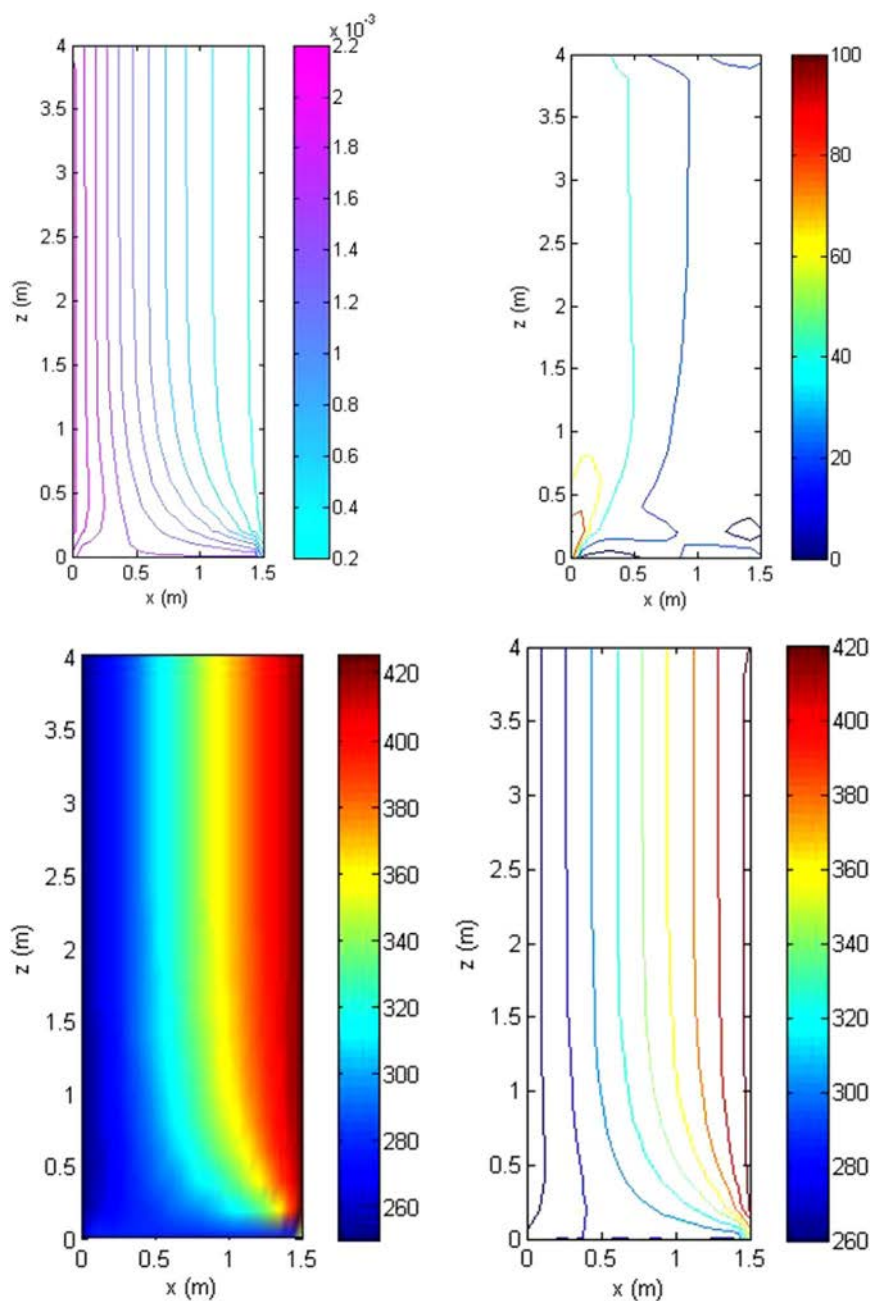


Fig. 6. A 2-D cylindrical fluidized bed reactor model for hydrochlorination of Si as proposed by Wang [35]. Two-dimensional slices extending from the central cooling tube to the reactor wall are shown (with x indicating radial direction and z the axial direction). Top row: Temperature distribution (°C) with both surface and contour diagrams. Bottom row: Instantaneous reaction rate distribution for TCS production (mol/s) and particle size distribution (μm).

MATLAB was used to implement the modified K-L model based on Becker's kinetics for isothermal operation. There was generally good agreement with experiment, with the average difference from experimental values being less than 6%. For runs with HCl addition, its effect was simulated by doubling catalytically active iron content in the model. The authors then built a pilot scale reactor in a follow-up study and further modified the model by instead using Werther's bubble model [48] and allowing for temperature variation along the length of the reactor. Average difference between predictions and experiment was reduced to 3.3%.

3.1.3. Thermodynamic equilibrium distribution models

Ding et al. [36] studied thermodynamics of the reacting system present during the hydrochlorination of Si in the presence of STC to produce TCS. They used minimization of total Gibbs free energy to

determine the equilibrium compositions of the system. The total Gibbs function was a function of the number of moles (n) of each species and its chemical potential, with the chemical potential itself being a function of standard Gibbs free energy and fugacities. Gas phase species were assumed to behave as ideal gases. This function was then minimized to determine the set of n values using MATLAB software. This procedure involved choosing reactants and their relative proportions, choosing products, choosing operating temperature and pressure and then performing the minimization. The authors assumed the system consisted of STC, H₂, Si, TCS, DCS and HCl species based on experimental observations. The calculations used operating conditions with temperatures of 373–873 K, pressures of 1–20 atm and H₂/STC molar feed ratios of 1–5. At the same time, equilibrium STC conversions and TCS selectivity were calculated for each set of parameters. The two-step hydrogenation-hydrochlorination reaction of the Si

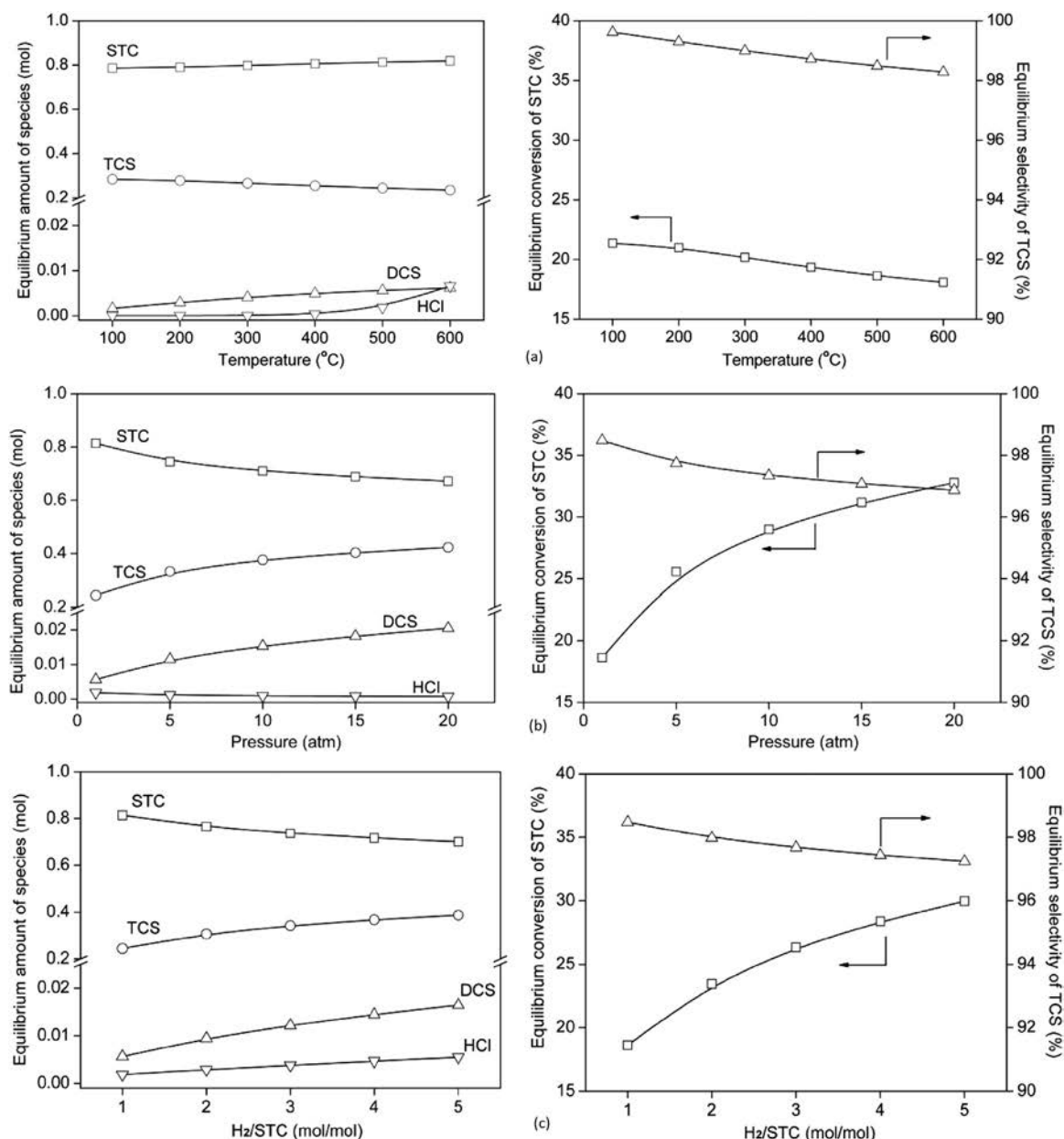


Fig. 7. Equilibrium composition (STC, TCS, DCS, HCl), STC conversion and TCS selectivity for (a) varying temperature, (b) varying pressure and (c) varying H₂/STC molar feed ratios from Ding et al.'s work [36]. Reprinted (adapted) with permission from [36]. Copyright (2014) American Chemical Society.

reaction system was considered consisting of a gas phase conversion of STC reaction which produces HCl and a gas-solid reaction in which HCl reacts with Si with both reactions also producing TCS. The stoichiometries of these reactions were then used to calculate the heats of reaction, gibbs free energy changes and reaction equilibriums for each of the two individual step reactions and also their combined overall reaction.

The results of the calculations can be seen in Fig. 7. The STC hydrogenation reaction was found to be endothermic and equilibrium limited, while Si hydrochlorination reaction was found to be exothermic and irreversible and the combined reaction was essentially thermally neutral. The equilibrium constant for the overall combined system is orders of magnitude higher than for homogenous STC hydrogenation and increases TCS yield. For simulated temperatures, TCS was the dominant product with trace amounts of DCS and HCl. STC conversion decreased slightly with increasing temperature while DCS increased. HCl formation was suppressed below 673 K and was started above 773 K, resulting in slight drop in TCS selectivity from

99.7% at 373 K to 98.5% at 873 K. TCS was also dominant over the entire simulated pressure range. STC conversion increased markedly with increasing system pressure. DCS production increased with pressure, which in turn decreased TCS selectivity from 98.1% at 1 atm to 96.8% at 20 atm. HCl production was suppressed at higher pressures. TCS continued to be the dominant species over the range of H₂/STC molar feed ratios, with only trace amounts of DCS and HCl produced. Increasing H₂ increased STC equilibrium conversion and enhanced TCS yield. It also increased DCS and HCl somewhat, in turn decreasing TCS selectivity.

The thermodynamics of the hydrochlorination of Si in the presence of STC were also investigated by Wu et al. [37]. However, they worked with seven reactions occurring in the system involving STC, H₂, Si, TCS, DCS, SiH₃Cl and HCl as chemical species. The Gibbs free energies and subsequently equilibrium constants for each reaction were calculated in the temperature range 473–1073 K. Here results agreed with Ding et al.'s work in which the combined hydrochlorination reaction has a decreasing equilibrium constant

with increasing temperature. The authors then reduced reactions to four independent reactions using the Brinkley method [49] and obtained four mass equations. These equations related molar amounts of chemical species to their equilibrium constants. Utilizing conservation of mass and initial molar amounts of reactants, the equilibrium composition of gaseous species were calculated for system pressures of 0.1, 1 and 5 MPa and STC/H₂ molar feed ratios of 1, 1/2.5 and 1/5. H₂ was found to have the highest equilibrium molar fraction in the system across all conditions, with fractions of H₂, STC and TCS decreasing with higher temperature and those of other species increasing (with HCl markedly increasing above 900 K). Increasing system pressure also increased TCS molar fraction. On the other hand, increasing H₂ in the feed decreased TCS molar fraction at equilibrium. STC conversion was found to increase with greater system pressure and initial H₂ and lower temperature.

3.1.4. Hydrogenation of STC without MG-Si

Kuniohi et al. [38] looked at the hydrogenation of STC to TCS without the presence of MG-Si. They attempted to capture many elementary reactions beyond the handful usually studied (as seen in previously listed literature in this section) by looking at literature for silicon CVD (Chemical Vapor Deposition) chambers. They based their reaction model on one proposed by Ravasio et al. [50] and after adding reactions from multiple other sources ended up with a total of 63 reactions comprising 26 chemical species. Only the forward rate coefficients were adapted from these sources, sometimes obtained by fitting with temperature data, while reverse rate coefficients were obtained from equilibrium constants. The entire system was simulated taking place in ideal 1-D plug flow reactor divided into two parts: a first section involving hydrogenation of STC at constant high temperature and a second section representing a cooling process in which the temperature was brought down to 300 K (decreasing linearly with position along the length of the reactor). The system was simulated at atmospheric pressure and the varied parameters were the temperature (1073, 1173, 1273, 1373, 1473 and 1573 K) in the first reactor section, feed STC/H₂ ratio (1:1, 1:2, 1:3 and 1:4) and cooling rate (−12.73 and −50.92 K/cm). The distribution of chemical species along the reactor was calculated using CHEMKIN-PRO. This software suite solved conservation of mass equations for each species after reaction with the aid of conservation of total mass.

For the STC hydrogenation step, the system reached equilibrium at 1273 K and above while it did not do so for lower temperatures. For these equilibrium conditions, the products were mainly TCS, HCl and SiCl₂. With increasing temperatures, the mole fractions of SiCl₂ increased and those of TCS decreased. In the cooling step, none of the studied cases indicated having reached equilibrium, while the TCS mole fraction increased for all of them with higher hydrogenation temperatures producing higher TCS mole fractions. The main reaction with the highest rate was SiCl₂ (g) + HCl (g) → SiHCl₃ (g). Although many of the other reactions had much smaller reaction rates individually, their sum produced an impact on the whole process and reduced efficiency by destroying TCS or producing STC. Sensitivity analysis concluded that a higher temperature for the hydrogenation step resulted in a lowered efficiency of STC conversion to TCS. For all cases of the cooling step, SiCl₂ eventually vanished to final mole fraction of 1 ppm or below. Once this happened, with this occurring in a shorter length for higher cooling rates, no other reactions proceeded at appreciable rates. Overall, the cooling step increased TCS production efficiency, with higher cooling rates producing better results. The best STC to TCS conversion efficiency was obtained at 1473 K, with a feed STC/H₂ molar ratio of 1:4 and cooling rate of −50.92 K/cm. The authors concluded that their reaction model agreed well with previous experimental results but that some reactions may exhibit strong pressure dependences. Hence, operating pressure a variable which should be further investigated.

3.2. Production of silane through reactive distillation

Huang et al. [51] studied the production of silane through disproportionation of TCS using reactive distillation (RD). The three main catalytically assisted reactions involved in this process are the following:



The rate equation for each of these reactions follows second order kinetics. The reaction rate constants and equilibrium constants for each reaction were calculated over the temperature range 273–373 K using Arrhenius and Van't Hoff based relationships. The third reaction, producing silane, had both the highest kinetic and equilibrium constants. Even with pure TCS being fed into the system, the very low equilibrium constant of the first reaction results in an extremely low silane yield of 0.2%. This demonstrates the advantage of RD like processes as this reaction could not be practically run using a single reactor. Thermodynamic calculations, including a vapor liquid equilibrium model, were performed using Aspen Plus software with the built in Peng-Robinson equation of state selected. Binary interaction coefficients for chlorosilanes, missing from the Aspen Database, were imported from NIST ThermoData Engine. Half of the binary interaction coefficients of the system were not available and kept at the default zero value.

A typical RD column with three sections (stripping at the bottom, reaction section in the middle and rectifying section at the top) was investigated first. The reaction section was packed with solid catalyst which also functions as mass transfer internals with both coupled reaction and separation by distillation taking place at the same sites. Silane was the lightest component (lowest boiling point) and could be obtained as an overhead product while the heaviest STC could be obtained from the bottom. This study used Amberlyst A-21 anion amine ion-exchange resin as catalyst with particle sizes in range of 0.3–1.2 mm. The authors chose to use the equilibrium stage (EQ) model for distillation calculations and the RadFrac module in Aspen Plus to compute the steady state reactions. A 60-stage column was simulated where the top condenser was defined as stage 1. The reaction section was from stage 16 to stage 45, with a liquid residence time of 2.5 s on each stage defined as hold-up/liquid-flow-rate. The column was operated at a top pressure of 5 atm with a pressure drop through each stage of 0.5 kPa. The molar distillate to feed ratio was set at 0.25. TCS at 10 kmol/h was fed into the column on stage 46 (just below the reaction section) at 195 K and 5.5 atm.

The authors aimed for a silane purity of over 99%. For the typical RD column this was calculated to require a reflux ratio of 63 and a top stage temperature of 185 K. In order to reduce the energy load required to produce these conditions, a second RD column was simulated with the introduction of an intercondenser between the reaction section and rectifying section operating at a temperature of 258 K. This causes the heavy TCS and DCS components to be condensed and return to reaction section before reaching the rectifying section. This did not significantly affect the reaction section but increased concentration of silane in the rectifying section (12% in stages 5–15 opposed to nearly zero before) while reducing top condenser load by 97%. A second intercondenser, operating at 338 K, was added in the middle of the reaction section to reduce the cooling duty of the first intercondenser (50% reduction) and although it raised reboiler duty this would normally end up reducing overall energy costs as low-pressure steam is cheaper than electrical refrigeration units. The TCS disproportionation reaction now took place mainly below the second intercondenser. Fig. 8 gives the composition and reaction rate profiles for the RD column with two intercondensers.

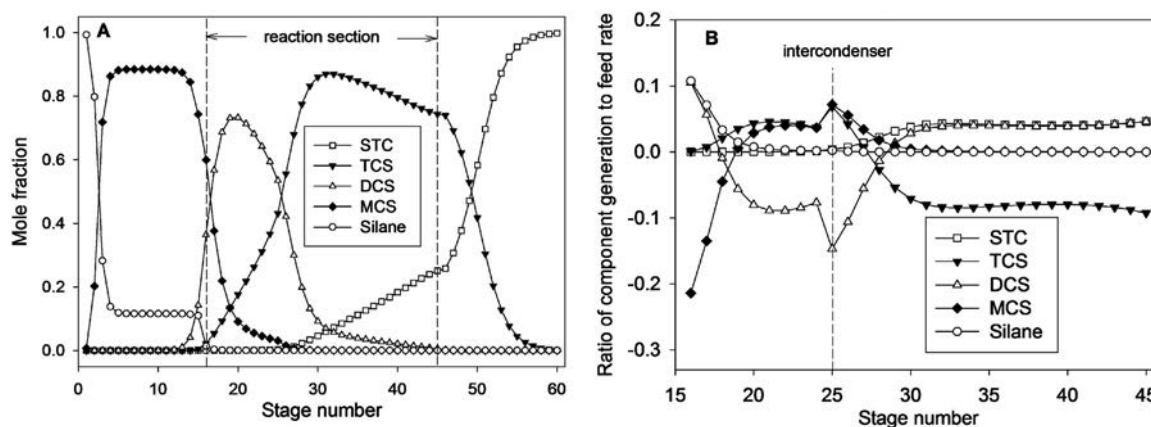


Fig. 8. Profile of reactive distillation column with two intercondensers. (A) liquid compositions; (B) generation rates. Reprinted (adapted) with permission from [51]. Copyright (2013) American Chemical Society.

In terms of parametric studies, for one intercondenser, it was found that the higher the location of the condenser is, the higher silicon purity and lower condensation temperature will be. Lowering the second condenser also lowers required condensing temperature. Increasing the duty of either condenser increases silane purity. Increasing pressure from 5.0 to 6.5 atm raises reaction temperature and increases reaction rate and silane purity. However, increasing pressure beyond 7.0 atm decreases silane purity as equilibrium conversion of SiH_3Cl (MCS) in exothermic reaction is decreased. Decreasing the residence time requires a greater number of stages to reach the same purity. Optimization places the two condensers between the rectifying and reaction sections within stages 22–26 and the residence time should be between 2–4 s.

Shuaishuai and Guoqiang [52] also looked at silane production, first in a RD column and then a two column RD process. The same set of three reactions as used by Huang et al. above were modeled as second order reversible reactions with rate and chemical equilibrium constants determined as functions of temperature based on Arrhenius and Van't Hoff equations. The RD column consisted of 60 stages; 15 rectifying, 30 reactive (with DOWEX MWA-1 as catalyst) and 15 stripping stages. Chemical reactions were assumed to occur in liquid phase only. Total effective liquid holdup was 300 L evenly distributed among reaction trays, TCS was fed into the system in the middle of the reactive section (stage 19) at 353 K and overhead pressure was 350 kPa in the column. Simulations were carried out using Aspen Plus with the RadFrac block based on EQ model with the aim of achieving 99.9% silane purity.

The required reflux ratio was found to be 46.11 with a condenser temperature of 216.23 K. Operating pressure was changed between 300–400 kPa which caused increases in temperature, with the authors concluding 350 kPa was most suitable as operating pressure. Moving the feed stage location down from the top charged condenser duty little until stage 19, below which the duty started to increase. Hence, optimum feed stage was set as 19. Increasing the liquid holdup beyond 4 L was found to dramatically decrease boil-up and reflux rates. Based on intermediate condensers in previous studies, a pumparound block (withdrawing vapor, condensing it in an external heat exchanger and then returning the liquid to the column) was tested at various locations on the column. Optimal locations had vapor withdrawn on stage 19 and liquid returned at 16, resulting in reduction of condenser duty by 82.88%.

In order to avoid the extremely low refrigerant temperatures required for the single RD column and operate with temperatures above 223 K, a double column process was simulated. This involved withdrawing a liquid stream from the top of the first column and passing it into a second high pressure distillation column to produce high purity silane and recycling the bottom product of the second column (with unreacted reactants) back to the first column. The second

column had an operating pressure of 3 MPa and 7 stages with feed at 4th stage. The content of DCS, MCS and silane in the first column was specified as 99.9% and STC in bottom product was also set to 99.9%. The condenser temperature could be increased to 268 K by moving the recycle stream position in the first column up but this also increased condenser duty. The authors concluded that the recycle stream should be located between stages 14–18.

Alcántara-Avila et al. [53] expanded on the intercondenser based work of Huang et al. [51] by using the same chemical reactions, catalyst and operating conditions but investigating an increased number of locations for heat exchange (both intercondensers and interboilers) within the column. The objective was set as minimizing operating cost based on heat exchanger loads while still obtaining greater than 99% purity silane. Locations for condensers using refrigeration or cold water cooling were considered for the top half of the reaction section and above while locations for steam based reboilers were considered for the bottom half and below. Changes in condenser and reboiler duties due to heat integration at stages were predicted through use of compensation terms [54]. The log mean temperature difference, used to determine temperature driving force for heat transfer in exchangers, was used as a feasibility criterion for heat integration using Big-M method. Aspen Plus with RadFrac was used to model the RD. Simulation software was used to first find optimal values of continuous variables and then an optimization software was used to find optimal values integer variables relating to locations of intercondensers and/or interboilers.

The column itself consisted of 62 stages. TCS was fed into the middle of the reaction section at stage 16. For all cases, it was found to be optimal to only have the regular reboiler at the bottoms with no other reboilers at any location. For the case with one inter-condenser (refrigeration based), its optimal position was found to be at stage 10 (in rectifying section) with a load of -433 kW (reducing the load of the top reflux condenser from -456 kW in conventional case to -23 kW) and overall operating costs (OC) reduced from $\$801,874/\text{yr}$ to $\$347,435/\text{yr}$. For two inter-condensers, one was placed at stage 4 (rectifying section) with duty of -105 kW (refrigeration) and another was placed at stage 25 (reaction stage) with duty of -450 kW (cooling water) while reflux condenser duty remained at -23 kW but reboiler duty now increased to 619 kW from 496 kW in previous two cases. For the last case OC decreased to $\$325,346/\text{yr}$ but equipment costs increased to $\$492,375$ from $\$387,988$ for one inter-condenser and $\$390,980$ for conventional. The case with two inter-condensers, with both installed above the feed stage, lowered the temperature profile which increased intermediate species concentration and ultimately boosted silane generation.

Zang et al. [55] on the other hand pursued lower costs through the introduction of additional reactive sections in a single distillation

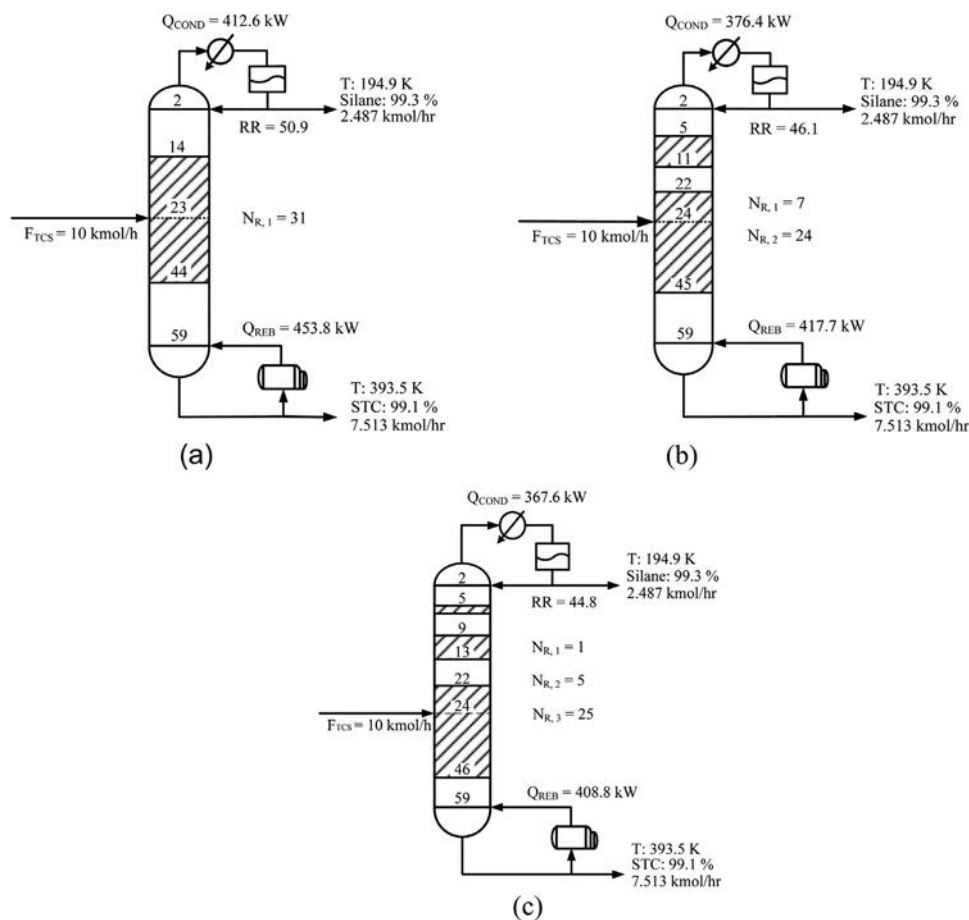


Fig. 9. Optimized reactive distillation column designs with (a) single reactive section, (b) double reactive sections and (c) triple reactive sections. Reprinted with permission from [55]. Copyright 2017 American Chemical Society.

column. Steady state operation was investigated for columns with one, two or three reactive sections. The total number of stages, number of reactive stages (distributed among the number of design specified reactive sections) and operating conditions were kept constant for each column. Aspen Plus with the *Rac-Frac* module and Peng-Robinson equation of state was utilized for simulations. The condenser heat duty was chosen as the metric for design comparison and optimization. Column layout was found used a simple grid-search method and the number of stages in the separating sections and feed location of TCS were employed as structural decision variables. The optimized stage locations and heat duties for each design are shown in Fig. 9. Increasing the number of reactive sections decreased both condenser and reboiler heat duties, with the triple reactive section design achieving 10.91% and 9.92% reductions respectively. Side condenser additions were also tested and found to be best located in each of the separating sections above the TCS feed.

Li et al. [56] built on the earlier study of Huang et al. [51] by instead looking at a single RD column with intermediate condensers and the addition of two purification columns in series downstream of the RD. Aspen Plus with Peng-Robinson equation of state and binary interaction coefficients derived in the earlier study were used. The RD unit was split into two separate columns for the purposes of modeling, with the stripping and reaction section as one column connected by an intermediate condenser to the rectifying section as a second column. For testing a second intermediate condenser, it was located in the reaction section of the first column as side-cooling duty. The overhead vapor of the second (rectifying section) column was then run through the first purification column to remove light fraction and the last purification column to remove heavy fraction. The final column overhead was required to produce 99.9999% ultrapure silane. The authors

sought to use overall operating cost, based on the two-factor utility cost equation of Ulrich and Vasudevan [57], as an optimization parameter. The best design was found to use a single intermediate condenser with a rectifying section overhead condenser temperature of $-40\text{ }^{\circ}\text{C}$ producing 82% pure silane (as opposed to the $-78\text{ }^{\circ}\text{C}$ required for above 99% from previous studies). Hence, the secondary purification columns allowed the reduction of energy duties for the rectifying section overhead.

4. Deposition of Si Based compounds to form SOG-Si

A very brief overview of models for Si deposition for PV applications is provided by Nie et al. [58], where they classify models as transport controlled, chemical reaction rate controlled and mixed transport-kinetic controlled.

4.1. Trichlorosilane deposition in bell jar reactors

An overview of the studies which specifically model TCS in bell jar reactors is presented in Table 2.

Ni et al. [59] developed a model to model Si CVD in Bell Jar Reactors. They employed Favre averaged equations for steady-state gas flow involving conservation of momentum, energy and mass with numerical method operative conditions given in Fig. 10. These were closed by a turbulence closure model. Turbulence-chemistry interactions were modeled by Eddy-Dissipation-Concept (EDC) model [60]. Radiative heat transfer was incorporated using discrete ordinates radiation model [61]. The non-linear partial differential equations were iteratively solved using Ansys FLUENT. A reaction model of the system was adapted from Balakrishna et al. [62] along with a set of

Table 2

Modeling studies of TCS deposition in Siemens Bell Jar Reactors. All models solve the standard continuity, momentum, energy and transport equations.

Study	Model Type and Techniques	Software	Reaction Model & Kinetics Source	Salient Features
Del Coso et al. [68]	2D, laminar flow, 1 rod	not specified	Habuka et al. [70]	tested effect of <ul style="list-style-type: none"> •pressure •gas composition •rod surface temperature •gas inlet temperature
Huang et al. [66]	3D, turbulent, 12 rods	FLUENT	Habuka et al. [70]	<ul style="list-style-type: none"> •novel design with bucket covering rods •plug flow in bucket •compared with identically sized conventional design
Ni et al. [59]	2D & 3D,RNS, Eulerian, DO radiation, Eddy-Dissipation-Concept (EDC), turbulent flow, 12 rods	CHEMKIN, FLUENT	modification of Balakrishna et al. [62] with some parameters from Cavallotti and Masi [71]	<ul style="list-style-type: none"> •2D single wafer reactor modeled with CHEMKIN & FLUENT to confirm reaction kinetics before full 3D in FLUENT •effect of different rod diameters
Ni and Chen [63]	3D, RNS, Eulerian, DO radiation, EDC, ISAT, turbulent flow, 12 rods	FLUENT	Ravasio et al. [50] for gas phase, Balakrishna et al. [62] for surface	tested effect of <ul style="list-style-type: none"> •effect of 3 different gas phase reaction mechanisms •effect of different rod diameters
Huang et al. [69]	3D, 12 rods	FLUENT	Habuka et al. [70]	<ul style="list-style-type: none"> •novel design with 2–3 reactors connected in series •exhaust gases of prior reactor fed into inlet of next •effect of molar fractions and pressure

Variables	Operative conditions
Pressure–velocity coupling:	Simple
Pressure discretization:	Standard
Momentum discretization:	Second order upwind
Energy discretization:	Second order upwind
Reacting species:	Second order upwind
Near-wall treatment:	Standard wall functions
Under-relaxation factor:	Pressure: 0.3, density: 0.8, momentum: 0.5, turbulent kinetic energy:0.8, turbulent dissipation rate:0.8, turbulent viscosity: 0.8, reacting species: 0.8, energy: 0.9

Fig. 10. Numerical method used to solve governing equations by Ni et al. [59].

semi-empirical surface reactions. Simulations of deposition rates were then validated using first CHEMKIN software followed by FLUENT, with both models having closely matching predictions and matching experimental data after modification of the kinetic model. This was followed by a 3D Eulerian frame CFD simulation of a 12 rod Siemens bell jar reactor of three different rod diameters using FLUENT coupled with the modified reaction kinetics model.

Obtained gas velocity and rod temperature distributions can be seen in Figs. 11 and 12. Increasing rod diameter decreased rod surface temperatures and heating flux provided to the rod surface. For the 50 mm rod, Si deposition is controlled by gas species transport, for 80 mm surface reaction rates and gas species transport control Si deposition and at 100 mm surface reaction rates control deposition rate. Ni and Chen [63] further looked at a similar system using the same governing equations and reaction model, solving them using the SIMPLE algorithm [64] iteratively with FLUENT and in-situ *adaptive tabulation* (ISAT) [65] to accelerate chemistry calculations. A six rod reactor was simulated with three different rod diameters with a focus on effects of gas phase reaction mechanisms. Silicon growth rates decreased with increasing HCl concentration at rod surface while STC formation did not affect growth rates.

Huang et al. [66] studied the deposition of Si from TCS in order to design an improved Siemens bell jar based reactor. This novel reactor consists of a bucket within the traditional bell jar shell; this bucket covers the inlet holes opening into the reactor and the bucket has small opening on the top allowing exit of gases which then exit from openings on the floor of the reactor (as is normally the case) outside the bucket. In this manner the flow inside the reactor can be easier to control plug flow as opposed to the chaotic mixed flow in the conventional reactor with both input and exit openings in the same chamber. The governing Eqs. (11)–(17) used to model the systems are the following:

Continuity equation:

$$\nabla(\rho U) = S \quad (11)$$

where the source term, $S = R_{Si}$ is the polysilicon deposition rate on the rods.

Momentum equation:

$$\nabla(\rho U U) = -\nabla P + \rho \mathbf{g} + \nabla \left[\mu(\nabla U + (\nabla U)^T) - \frac{2}{3} \nabla U \right] - \nabla(\rho \overline{\mu' \mu'}) \quad (12)$$

Transport equations for standard $k - \epsilon$ model:

$$\nabla(\rho U k) = \nabla \left[\left(\mu + \frac{\mu_t}{\sigma_k} \right) \nabla k \right] + G_k + G_b - \rho \epsilon \quad (13)$$

$$\nabla(\rho \epsilon U) = \nabla \left[\left(\mu + \frac{\mu_t}{\sigma_k} \right) \nabla \epsilon \right] + C_{1\epsilon} \frac{\epsilon}{k} (G_k + C_{3\epsilon} G_b) - C_{2\epsilon} \rho \epsilon \frac{\epsilon^2}{k} \quad (14)$$

Energy equation:

$$\nabla((\rho E + p)U) = \nabla(\lambda_{eff} \nabla T) + S_h \quad (15)$$

where the source term, $S_h = \nabla \cdot (I(r, s)s)$, is the increment of radiation intensity in direction \mathbf{s} .

Radiative transfer equation:

$$\nabla \cdot (I(r, s)s) + aI(r, s) = a \frac{\sigma T^4}{\pi} \quad (16)$$

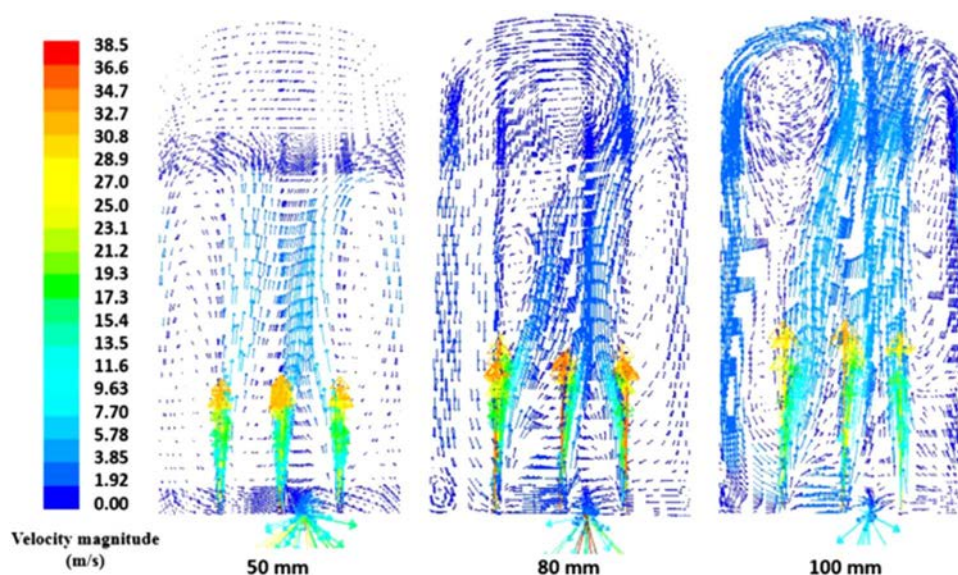


Fig. 11. Gas velocity distribution in bell-jar reactor with 12 rods of three different diameters from 3-D CFD simulations of Ni et al. [59].

Species transport equations:

$$\nabla(\rho \mathbf{U} Y_i) = -\nabla J_i (i = \text{HCl}, \text{H}_2, \text{SiCl}_2\text{H}), J_i = -\rho D_{i,j} \nabla Y_i \quad (17)$$

Simulations were carried out using Fluent to solve governing equations with the SIMPLE method for pressure-velocity coupling and meshes generated using GAMBIT. For model validation, the outlet temperature for conventional reactor was found to deviate 10% from industrial data. Profiles of velocity, temperature and concentration are shown in Fig. 13. The velocity in the novel reactor was more uniform (plug flow) while the traditional reactor had much higher velocity near the bottom and a dead zone near the top. The traditional reactor had higher local temperature near the top, despite appearing to have a more uniform temperature field, likely caused by the flow dead zone observed for velocities. The elimination of this in the novel reactor should inhibit formation of silicon powders, in turn reducing wall contamination and heat loss. The traditional reactor shows more uniform mass fraction distribution of TCS due to its mixed flow pattern, although there is reduced mass fraction near the top due to dead zone again. The overall energy loss and hence power consumption of the novel reactor was found to be lower than the traditional reactor with increasing rod diameter. This is presented in more detail in a separate paper by the authors [67] discussed in Section 4.6.

A model for CVD in a TCS and H_2 system for a single rod was

developed by del Coso et al. [68]. The transport and conservation equations were simplified under the assumptions of no axial diffusion of properties, steady and laminar flow, ideal gases, that gas transport properties are independent of mass fractions, that thermal diffusion and viscous energy dissipation are negligible and the pressure is constant. The kinetics were modeled by splitting the second-order overall deposition reaction into two single order systems. Increasing reactor pressure, rod surface temperatures and gas inlet temperatures increased silicon growth rates.

Huang et al. [69] sought to reduce the cost of the Siemens approach and increase TCS conversion efficiency by proposing to connect multiple bell jar reactors in series. The exhaust of the first reactor, typically high in unconverted and wasted TCS, is instead fed directly into the next reactor's inlet after cooling. Fully 3D quasi-steady state simulations were carried out using Fluent software with standard continuity equation, momentum equation, standard $k-\epsilon$ transport model equation, energy equation and inclusion of radiative transfer equation. Chemical kinetics were based on Habuka et al.'s [70] model for epitaxial growth of silicon from TCS decomposition on a hot surface. The two reactor configuration was found to reduce production costs by 21.9% compared to a single reactor, while a 3 reactor process lowered costs by 26.9%. Increasing pressure also reduced costs while increasing average growth rate. However, lowest costs were observed at 9.1% TCS

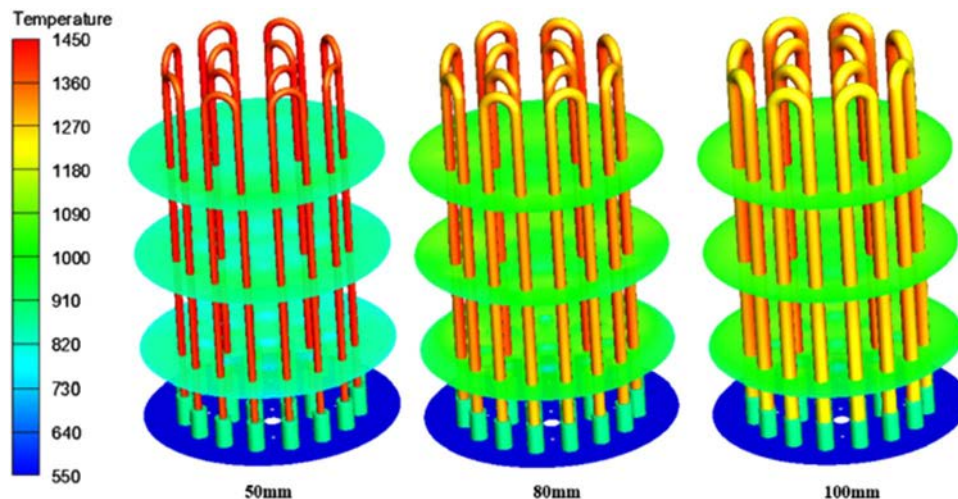


Fig. 12. Rod temperature (K) distribution in bell-jar reactor with 12 rods of three different diameters from 3-D CFD simulations of Ni et al. [59].

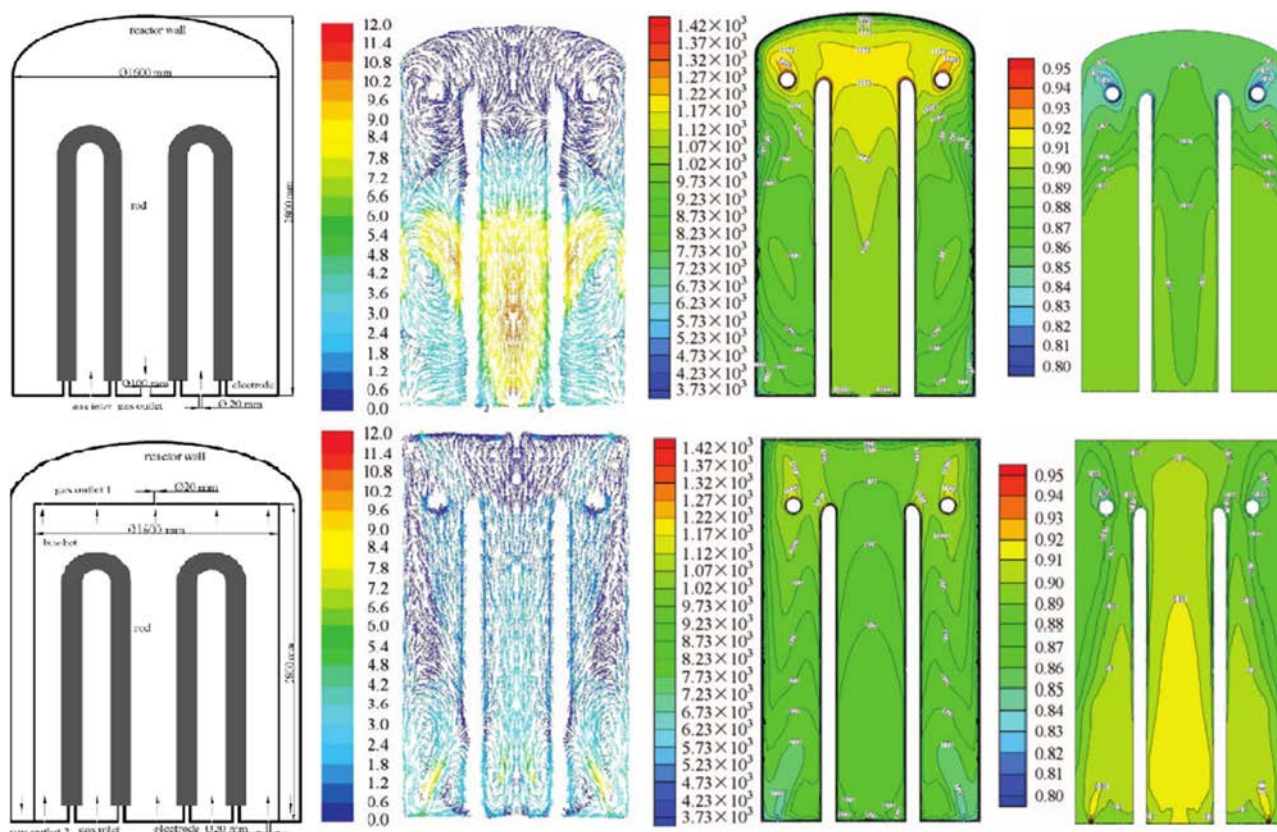


Fig. 13. Comparison of conventional bell jar reactor (top row) with novel modified bell jar (bottom row) proposed by Huang et al. [66]. The first column shows schematics of the designs, the second column compares gas velocity vectors (m/s), the third column compares temperature distributions (K) and the fourth column compares mass fraction profiles of TCS. Reprinted with permission from [66]. Copyright 2013, The Electrochemical Society.

concentration in feed while highest deposition rate was at 25% concentration. Decreasing HCl in the second reactor from 10 wt% to 2 wt% also reduced costs by 35.5%.

Cavallotti and Masi [71] proposed a mechanism for Si deposition from TCS, utilizing reaction kinetic parameters from both literature and their own ab-initio calculations. They found that the net deposition rate of Si is the sum of the adsorption rate of gas precursors and the etching rate of HCl (working to reduce deposition). This mechanism was then implemented in 3D CFD where the mechanism reproduced experimental data and the Siemens reactor was found to operate in a mixed kinetic-transport controlled regime.

4.2. Trichlorosilane deposition in fluidized bed reactors

There is very little literature available on TCS use in FBRs, likely because the high decomposition temperatures needed and corrosive gas mixture make it less attractive than silane decomposition in FBRs [72]. Furthermore, the authors were unable to find any recent academic articles relating to modeling of TCS FBRs except the two studies presented in this section. Moon et al. [73] modeled a FBR utilizing TCS precursor (investigating flow behavior and not considering reactions) while looking at the effect of single and multi-jet nozzles. The nozzles are used to aim TCS at the reaction area to avoid the highly reactive TCS gas from contacting other parts of the vessel. Three configurations for nozzles were tested; a single large diameter nozzle at the bottom center of the vertical reactor and facing directly up and two different smaller diameter four nozzle configurations. A fully 3D unsteady CFD simulation was carried out using Fluent software based on the Eulerian-Eulerian model (described in more detail in Section 4.4 on silane FBRs). Lift forces were ignored and drag force was described by Syamlal-O'Brien model [74]. Pressure velocity coupling used PC-SIMPLE algorithm. Multi-block grids were utilized with more refined

grid near the nozzles. The simulations closely matched cold-model experimental results for the same setup. The single nozzle was found to strongly concentrate TCS gas in the reactor center, indicating low available gas-solid reaction area. The multi-jet nozzle configurations ensured better distribution and thus higher gas-solid contact area, with the smaller diameter configuration yielding 3.6 times greater contact area than single nozzle for regions with the same TCS concentration.

Li et al. [56] attempted to address the problem of TCS deposition on heated reactor walls in a FBR by proposing an internally circulating fluidized bed (ICFB). Their cylindrical design consisted of a central draft tube into which TCS was fed and which contained the reaction zone and an annulus region between the central tube and reactor walls which contained the heating zone. Polysilicon granules in the draft tube formed a riser bed where they rose to the top of the draft tube and fell over its edges into the annular heating zone by gravity. Once in the heating zone, the particles moved downward to form a high density downer bed. Here the particles were then able to flow back into the draft tube from the annulus through orifices, due to differences in solid holdup, and hence established a solid circulation cycle. This design was tested by the authors in a cold-test experimental setup [75] where fluidization of wide size distribution particles, bypass ratio from reaction zone to heating zone and solid circulation rate were calculated to fit requirements for polysilicon deposition without excessive silicon deposition in heating zone. The authors then attempted to computationally model this reactor system for the cold test conditions without reactions. Although such purely hydrodynamic behavior studies already exist for other systems, it was claimed that this was a unique ICFB design specifically for polysilicon production and such needed earlier computational results cannot be used.

Simulations in 2D were carried out with a two-fluid (Euler-Euler) model, granular kinetic theory, Johnson-Jackson model for friction viscosity, Gidaspow [76] and Syamlal-O'Brien drag model and standard

$k - \epsilon$ model. Finite volume technique with SIMPLEC algorithm was used for CFD simulations. Only air, nitrogen and glass beads (for solid phase) were simulated to match the cold-test experimental setup and no reactions were considered. Quad grids mesh was adopted with finer mesh near draft tube orifices and walls. The Syamlal-O'Brien model was found to give best results for large particles. Gas velocities in the tube and annulus were found to be optimum when higher than initial fluidization gas velocity and increasing annulus gas velocity beyond draft tube gas velocity or decreasing particle size too much was found to setup an improper reverse circulation pattern. Gas velocity ratios, particle diameters, orifice sizes and positions and cross-sectional area ratios of annulus and draft tube were optimized to ensure good gas bypass ratios from tube to annulus and vice versa and ensure good heat transfer while preventing excessive silicon deposition on heating zone wall.

4.3. Silane pyrolysis in bell jar reactors

Jung et al. [77] modeled silane decomposition in a four rod bell jar type reactor (each slim rod was placed inside an individual heating jacket cylinder). A steady state turbulence model with a realizable $k - \epsilon$ was used for flow pattern analysis. The governing equations were solved using FLUENT with SIMPLE used for pressure-velocity couples. The reaction was modeled as a surface reaction with both one-step ($\text{SiH}_4 \rightarrow \text{Si} + 2\text{H}_2$) and two step ($\text{SiH}_4 \rightarrow \text{SiH}_2 + \text{H}_2$ and $\text{SiH}_2 \rightarrow \text{Si} + \text{H}_2$) routes. Kinetic parameters were estimated by fitting to experimental data through trial and error. Increasing silane flow rate, temperature and rod diameter increased Si deposition rates.

Jeon et al. [78] modeled the same jacketed four rod system with ANSYS while looking at a greater range of rod diameters (6 different diameters ranging from 10 to 120 mm). They assumed constant silane concentration and used the overall one-step reaction. The same pattern of increasing Si deposition rate with increasing rod diameter and rod temperature was obtained. There was a consistent distribution difference between rod zone and top zone of the reactor for both temperature and silane mass fraction, with temperature being higher and mass fraction being lower in the top zone. Power consumption was found to linearly correlate with Si deposition rate, with the slope increasing with increasing rod diameter.

The effect of gas input nozzle designs for the same four rod bell jar systems was investigated by Kang et al. [79] also using ANSYS and the realizable $k-\epsilon$ turbulent model. The two nozzles, types A and B, are shown in Fig. 14. The type B nozzle resulted in greater Si deposition rates as it produced greater silane gas concentration on the slim rods. The type A nozzle produced a vortex gas stream which caused nonuniform deposition while the type B nozzle formed uniform

deposition around the slim rod as it uniformly enveloped the rods. The type B rod also displayed lower power consumption throughout the deposition process.

Li et al. [80] looked at cooled jacketed rods with a focus on minimization of homogeneous nucleation of silane (producing fines) and its possible contribution to rod growth. A traditional bell jar reactor and one with jacketed rods, both with 12 pairs of rods, were compared. Gas flow was calculated through the steady state Reynolds-averaged Navier-Stokes (RNG) equations along with the standard continuity, momentum, energy and mass equations. Turbulence was modeled through RNG $k - \epsilon$ model with standard wall function. The heterogeneous kinetics models of Hashimoto et al. [81], Iya et al. [82] and Furusawa et al. [83] were tested and Hashimoto et al.'s kinetics were found to best match an experimental single rod setup and used for further calculations. Homogeneous kinetics were based on the model of Furusawa et al. [83]. The adhesion and deposition of fines (generated from homogeneous nucleation) onto the rod surface was derived from kinetic theory. The deposition rate was based on local concentration and averaged thermal velocity of gaseous silicon.

Simulations were carried out using ANSYS Fluent with Coupled algorithm for pressure-velocity coupling and second-order upwind scheme. The cooling jackets formed separate flow channels for the feed gas around each rod with steady flow (providing lower gas collision and recirculation than the conventional reactor), lower temperatures and higher silane concentration near the rods. This led to suppression of fines formation and higher silane conversion. Silane conversion decreased with increasing inlet flow rate and increased with higher operating pressure while fines formation showed the opposite behavior.

4.4. Silane pyrolysis in fluidized bed reactors

An overview of the studies which specifically model silane pyrolysis in FBRs is presented in Table 3.

An early model of the silane pyrolysis FBR system was created by Praturi et al. [84] in 1977. They derived kinetic rate expressions for 8 elementary reaction steps involving mass transport of silane and hydrogen, homogeneous pyrolysis of silane, homogeneous nucleation of silicon, heterogeneous pyrolysis of silane, heterogeneous nucleation of silicon and silicon crystal growth. However, they were limited by lack of experimental data to obtain various constants or complete understanding of the reaction mechanisms.

Lai et al. [85] also accounted for both CVD of Si and fines formation through homogeneous nucleation. They considered two pathways for silicon decomposition; a first order homogeneous decomposition of silane into gaseous precursor of solid silicon and first order hetero-

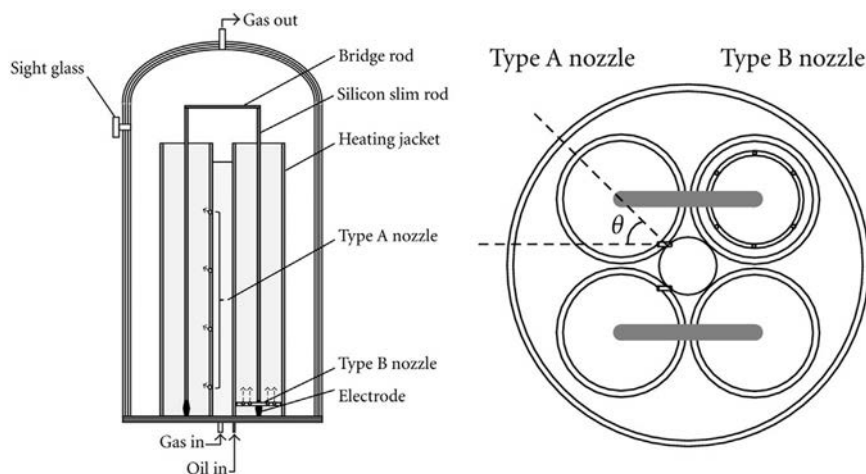


Fig. 14. Schematic demonstrating the two gas input nozzle designs (Types A and B) tested for silane decomposition in a bell jar reactor with heat jacketed Si rods by Kang et al. [79].

Table 3
Modeling studies of silane pyrolysis in fluidized bed reactors. All models solve the standard continuity, momentum, energy and transport equations.

Study	Model Type and Techniques	Software	Reaction Model & Kinetics Source	Salient Features
Guenther et al. [90]	2D & 3D, Eulerian-Eulerian	MFX	Furuwasa et al. [83]	grid independence tests; global and detailed chemical schemes tested; alumina seed particles; slightly varying temperatures
Xie et al. [91]	2D, Eulerian-Eulerian, ISAT	MFX	Fayolle [92] and Furuwasa et al. [83]	isothermal, alumina seed particles
Cadoret et al. [93]	2D & 3D, Eulerian-Eulerian, kinetic theory of granular materials, Schaeffer model [94]	MFX	Furuwasa et al. [83]	grid independence tests; alumina seed particles; differing powder mass, temperatures, silane mass fraction
Reuge et al. [95]	3D, Eulerian-Eulerian, SB drag law, kinetic theory of granular materials, Schaeffer model [94] and Princeton [96] model hydrodynamics, Rosseland radiative heat model [97]	MFX	Furuwasa et al. [83], Coltrin et al. [98–100] and Buss [101,102]	4 kinetic models test: one heterogeneous only and three combining homogeneous and heterogeneous reactions; incorporated silylene (SiH ₂) in gas phase to represent all reactive polysilanes
Balaji et al. [103]	multi-scale with 2D Eulerian-Eulerian CFD module, population balance module and CVD module	MATLAB, COMSOL	Lai et al. [85]	silicon particle growth based on population model (with scavenging factor) of White et al. [104]; heterogeneous reaction ignored; tested temperatures, inlet silane flow rate and mass holdup
Parker [105]	Computational Particle Fluid Dynamics [106–108] utilizing Lagrangian particle motion	Barracuda	Iya et al. [82], Hogness et al. [109]	tested two inlet gas distributors: uniform screen and nozzle; included scavenging reaction for fines; isothermal
Reuge and Caussat [110]	classical diffusion/reaction equations in porous media (chemical vapor infiltration) and Eulerian-Eulerian CFD	MFX	Furuwasa et al. [83], Coltrin et al. [98]	tested two models to study agglomerate formation during CVD, one analytical with stable particles and one dynamic with multi-fluid CFD
Du et al. [111]	multi-scale with Eulerian-Eulerian CFD module, population balance module and 2-phase reaction module	MATLAB, COMSOL	Iya et al. [82], Hogness et al. [109]	silicon particle growth based on population model (with scavenging factor) of White et al. [104] and Du and Ydstie [112]; tested silane inlet flowrate and concentration
Liu and Xiao [113]	3D, coupled Eulerian-granular and population balance modules	FLUENT	Hogness et al. [109] (HOG), Furusawa et al. [83] (FUR), Iya et al. [82] (IYA)	population balance module based on three node quadrature method of moments (QMOM) developed by Liu and Xiao [114] where particle growth is mainly by scavenging; gas phase global kinetics based on HOG & FUR while surface decomposition based on IYA & FUR

geneous decomposition of silane onto existing silicon seed particles. The concentration and growth of fines was modeled using a population balance model (PBM). This was applied to a fluidized bed bubbling reactor with bubble, emulsion and grid regions where gas and solids are well mixed. The calculations were compared to experiments at the Jet Propulsion Laboratory (JPL) [86,87], with the authors considering preliminary results in good agreement although there was overprediction of fines. Their model indicated less formation of bubbles and better gas-solid contact would reduce fines.

Hsu [88] characterized the JPL FBR experimental results and along with a follow up study [89] derived a silicon particle size growth model including mass balances with terms for homogeneous scavenging and heterogeneous CVD. They found that growth rate due to scavenging linearly increased with feed silane concentration. Furuwasa et al. [83] used experimental data from a fixed bed reactor to derive rate expressions, including conditions which produce CVD in interparticle spaces, applied to FBRs and claimed to better match experimental results than previous studies.

Guenther et al. [90] simulated FBRs using a two-fluid hydrodynamic model MFIX (Multiphase Flow with Interphase eXchanges [115]). These models, also called Eulerian-Eulerian models, treat fluid and solid as two continuous and fully interpenetrating phases. Mass, momentum and energy balance equations were constructed for both gas and solid phases in isothermal conditions. These partial differential equations were numerically solved using MFIX to find eight dependent variables in three dimensions: void fraction of gas phase, pressure of gas phase and six velocity components for both gases and solids. Governing equations were solved using finite volume method. Velocities were defined at cell faces using a staggered grid. The partial elimination algorithm [116] was used to uncouple discretized momentum equations due to gas-solid drag.

An extension of the SIMPLE [117] algorithm was used to iteratively solve the discretized equations and a solids volume fraction correction equation adjusted velocities in order to satisfy conservation of mass in both phases. Convective fluxes at cell faces were approximated using higher-order expressions through the Superbee method. During the silane deposition process, alumina (Al_2O_3) particles were used as seed particles in both experiments and simulations. Two chemical schemes were considered for the system. A global chemical scheme for the silane decomposition reaction $\text{SiH}_4 \rightarrow \text{Si} + 2\text{H}_2$ tracked two gas species and two solid species (including alumina). A detailed scheme involving the reversible reactions $\text{SiH}_4 \rightarrow \text{SiH}_2 + \text{H}_2$ and $\text{SiH}_2 + \text{SiH}_4 \rightarrow \text{Si}_2\text{H}_6$ and the irreversible reactions $\text{SiH}_4 \rightarrow \text{Si} + 2\text{H}_2$ and $\text{SiH}_2 \rightarrow \text{Si} + \text{H}_2$ tracked four gas species and two solid species.

For simulations, 25 and 80 cells were used in the radial and axial directions respectively and had been determined to be grid-independent in 2D. Grid independence is a qualitative measure for determining when grid independent average bed behavior has been reached instead of point to point convergence criteria. In order to test for this, several simulations were carried out first neglecting chemical reactions. Starting with a symmetrical 2D grid, the number of cells in the azimuthal z-direction was incrementally increased up to 36. For comparison with the high-order methods, a simulation with 24 z-cells was run using first-order upwinding (FOU). Simulations were run for 3.6 s and time averaged over the final 2.6 s. A qualitative change in bed expansion occurred with increase in number of z-cells upto a value of 12 after which it appeared to have converged. The FOU method was found to overpredict bed expansion. Grid independence was achieved for voidage profiles after 24 z-cells.

VOIDS/bubbles formed at the bottom of the bed were found to migrate towards the reactor center with time as they traveled upwards. In contrast, the 2D and FOU simulations predicted movement of voids away from the reactor center and significantly underpredicted solids concentration at the wall in lower bed regions. The full simulations with reaction were run with 24 z-cells for temperatures ranging from 871.55 to 882.45 K. Outlet H_2 concentrations predicted by the 3D

simulations very closely matched experimental results. There was found to be very little difference in results between the global and detailed chemical schemes, suggesting the dominant reaction mechanism is due to heterogeneous reaction.

The same system involving Si deposition on coarse alumina particles was studied by Cadoret et al. [93] using the MFIX code. This model can predict temporal and spatial evolution of local void fractions, gas and particle velocities, species gas fractions and silicon deposition rate. Calculations were performed using “the continuum model, the drag law of Syamlal-O’Brien [74], the kinetic theory of granular materials with an algebraic form for the granular temperature equation for solid phase stress tensor in the viscous regime, and the Schaeffer model [94] for solid phase stress tensor in the plastic regime.” A second order Superbee method was used to produce grid independence for both 2D and 3D simulations with 250 cells in axial direction (0.5 m height), 15 cells in radial direction and 6 angular cells (for 3D only). The chemical kinetics were assumed to follow the overall reaction of $\text{SiH}_4 \rightarrow \text{Si} + 2\text{H}_2$ with the following expression, from Furusawa et al. [83], for reaction rate:

$$R_{\text{SiH}_4} = (1 - \epsilon_g) \rho_g \frac{k_{s0}(6/d_p)}{1 + K_{\text{H}_2} P_{\text{H}_2} + K_{\text{SiH}_4} P_{\text{SiH}_4}} \frac{X_{\text{SiH}_4}}{M_{\text{SiH}_4}} \quad (18)$$

where k_{s0} is the reaction rate constant for reaction 3, the equilibrium constants K_{H_2} and K_{SiH_4} are given by [83], ϵ_g is volume fraction of the fluid phase, X_{SiH_4} is mass fraction and M_{SiH_4} is molar mass of silane.

There was marked difference between 2D and 3D results, see Fig. 15, especially with regards to void fraction which decreases monotonically from reactor center to wall while 2D results predict a maximum half way along the distance. In 2D, voids cannot cross the centerline boundary and are artificially reflected on this symmetric boundary condition. This demonstrates the importance of full 3D simulations and the deficiencies of 2D models. Increasing initial powder weight led to increased silane conversion. Fig. 16 shows the flow and conversion profiles for the reactor after 3.6 s. Two slugs of gas, one occupying most of the upper half and another from bubbles above the distributor, can be observed. These regions have low silane conversion (high silane mass fraction) while the regions in between have higher particle density and conversion (low silane mass fraction). Overall the model performs fairly well with a global deviation of 9% from experiments.

Reuge et al. [95] further carried out multifluid Eulerian simulations with MFIX and used the same governing equations as Cadoret et al. above. They sought to improve on previous studies through a better description of heat transfer in the bed by solving energy equations in two phases and implementing a model of Rosseland [97] for radiative transfer, testing two hydrodynamic models: the Schaeffer model previously used and the Princeton model [96], considering the sphericity of particles for available specific surface and implementing the Wilke approximation for multicomponent diffusion to better describe gaseous species transport. The same processing parameters and grid layouts were used as before (only 3D simulations). An extensive study of kinetic models available for the system was carried out and four were incorporated: the purely heterogeneous Furusawa model [83] (GC) and three models considering both homogeneous and heterogeneous chemistries from the works of Coltrin [98–100] (COL), Buss [101,102] (BUS) and Furusawa (FUR).

The authors acknowledge a limitation of the Eulerian models as they consider uniform species concentration at the particle which ignores local transport by diffusion and convection. While this is satisfactory for silane kinetics, it does not work well with silylene (SiH_2) and overestimates its consumption and reduces the role of polysilanes in the reacting system. It was then assumed that all the highly reactive polysilane species were present in gas phase as the highly reactive silylene. A comparison of (global time averaged)

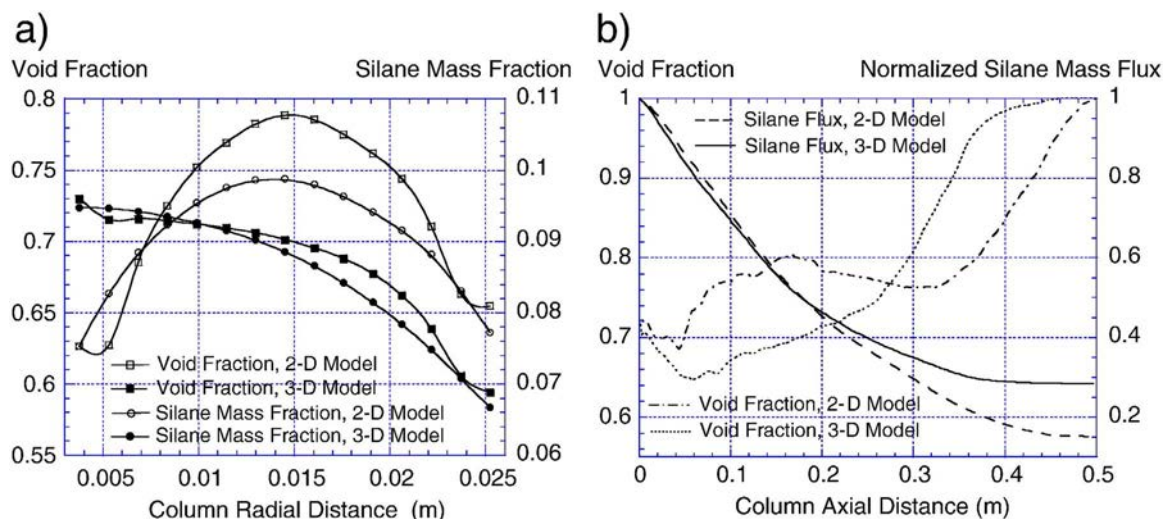


Fig. 15. Cadoret et al.'s [93] 2-D and 3-D simulation results for a fluidized bed reactor for silane pyrolysis showing (a) radial profiles of void fraction and silane mass fraction and (b) axial profiles of void fraction and normalized silane mass flux.

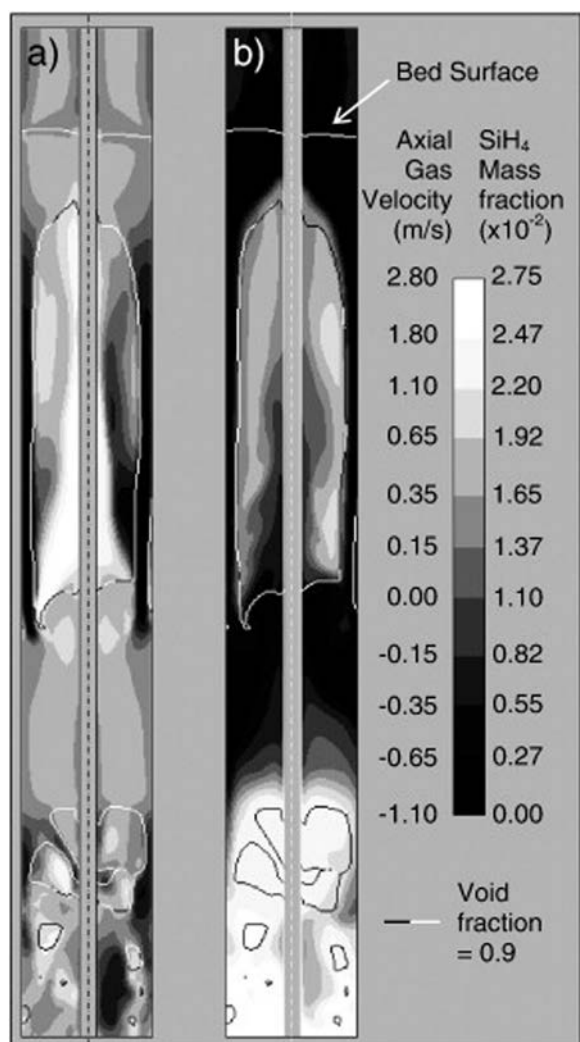


Fig. 16. Silane pyrolysis profiles for fluidized bed reactor after 3.6 s for (a) axial velocity and (b) silane mass fraction as produced by Cadoret et al. [93].

simulation results with experimental results is given in Fig. 17.

All runs required 15 s of process time to reach a temporally averaged pseudo thermal equilibrium over the bed. This was followed

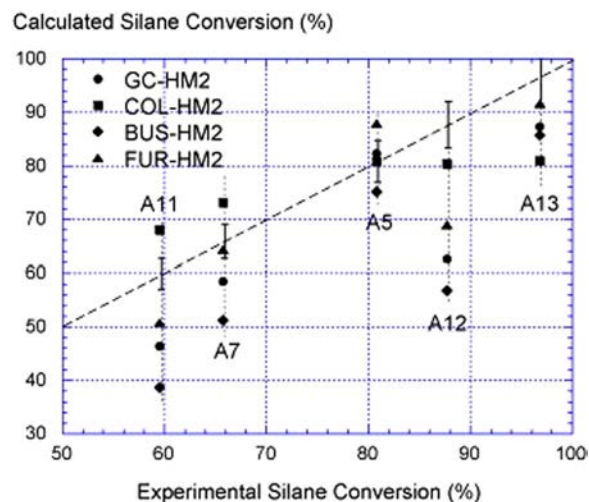


Fig. 17. Calculated silane conversions vs. experimental silane conversions for silane pyrolysis in a 3-D fluidized bed reactor modeled by Reuge et al. [95]. GC, COL, BUS and FUR are kinetics models (explained in text) and HM1 and HM2 are Schaeffer and Princeton hydrodynamic models respectively.

by an additional 8 s to account for gas-solid temperature fluctuations. Void fraction distribution followed similar patterns to that of previous studies with regions of gas slugs and regions of high particle density with corresponding low and high silane conversion respectively. Sharp concentration gradients at slug peripheries encourages diffusive transport in these regions. On the other hand, silane forms mainly in the gas rich slugs and leads to Si deposition in peripheral regions. However, a part of silane deposition can also occur in dense zones, as suggested by fixed bed simulations. The contribution of silane can be as high as that of silane locally. Increasing the inlet concentration of silane also increased Si deposition by silane.

Xie et al. [91] adapted in-situ adaptive tabulation (ISAT) [65], an algorithm utilized to help deal with complex systems of coupled nonlinear equations as found in many chemical systems. They applied it to control volume based two-fluid CFD for reacting multiphase flow for the first time, with isothermal silane pyrolysis in a FBR as their system. Kinetic constants for gas phase reactions were from Fayolle [92] while surface kinetics were obtained from Furusawa et al. [83] and Guenther et al. [90]. The MFIX code with SIMPLE algorithm was used for flow modeling. Computational efficiency and speed was found to increase when ISAT was used with a fixed time-step while a rapidly

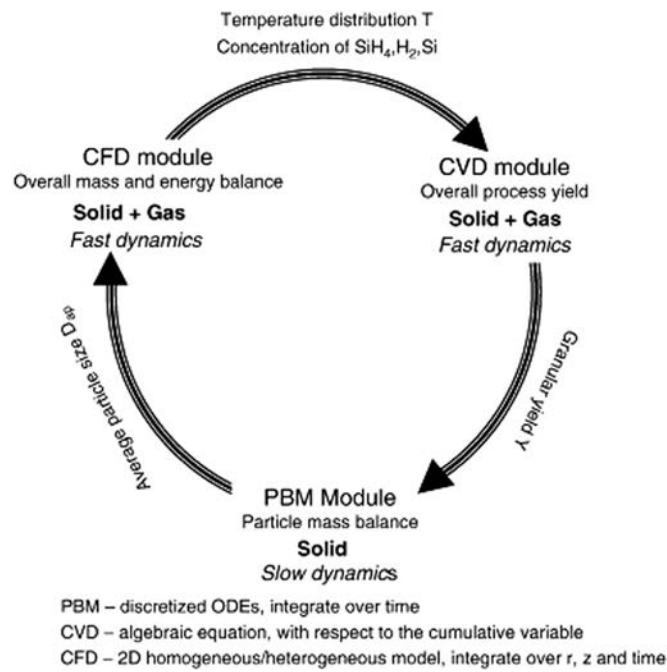


Fig. 18. Multi-scale model scheme employed by Balaji et al. [103] for Si CVD in a fluidized bed reactor, with three distinct but interacting modules.

varying time with time-splitting method did not increase performance.

White et al. [104] developed a population balance model for silicon particles in silane FBRs. They assumed particles grew by both heterogeneous CVD and scavenging from powder formed during homogeneous gas phase silane decomposition. Their model carried out size distribution of particles into discrete intervals based on particle mass and number. White et al. [118] then proposed using this population balance model in a multi-scale approach which coupled it with CVD calculations.

This work was then built-on by Balaji et al. [103], who carried out multi-scale modeling of the FBR which combined computational fluid dynamics (CFD) with population balance and chemical vapor deposition modules (Fig. 18). The CFD module provides reactor temperature and concentration at the vessel scale which are inputs to the CVD module. The CVD module calculates overall process yield which is an input to the population balance module. The population balance module calculates the average particle diameter which is then used as an input in the CFD module for further calculations. The population balance and CVD modules are solved using MATLAB while the CFD module uses COMSOL software and the interlink between both softwares is used to integrate the different modules.

The CFD module uses multi-phase flow equations used in the MFIX framework with the following assumptions: the void fraction along the bed was not solved explicitly as it reached steady state within a few time steps and so the entire bed is divided into n zones with constant volume fraction (3 in this study), particles are spherically and uniformly distributed in a zone and Si seed particles and their growth is modeled as solid phase and fine Si powder formation is regarded as silicon concentration in gas phase. The homogenous reaction rate expression, with the heterogeneous reaction rate being ignored as it does not play a significant role, is the following:

$$R_{hom} = 2e13 \frac{-26000}{T_g} c_{SiH_4} \quad (19)$$

where T_g is the gas phase temperature.

Silicon particle growth is modeled using a scavenging factor determined from the fraction of powder (produced by the above reaction) deposited on particles. The rate of scavenging is assumed

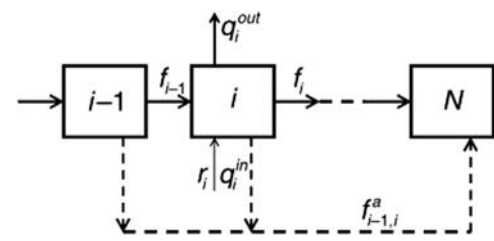


Fig. 19. Size interval characterization of particles in the population balance model of White et al [118] used by Balaji et al. [103] in their population balance module in Fig. 18.

proportional to reaction rate and total surface particle surface area. The population balance assumes that particles are distributed among N size intervals characterized by an average number of moles per particle. Deposition onto particles causes them to grow from one size interval to the next. The forces controlling this include addition of seed particles or withdrawal of product q_i , flow of particles from one interval to the next f_i and material transfer from precursor to particle substrate r_i as shown in Fig. 19. All of this assumes that the particle phase is well-mixed on the time scale of particle growth.

From the results of silane and product gas concentration profiles along bed length, most of the reaction was found to take place in the center as the reactor is heated above ignition temperature. Steady state was reached within a few times steps (30 s). Overall yield was found to decrease with time, likely due to void fraction decreasing as silicon hold up increases. Particle diameter at exit was found to strongly depend on void fraction, silicon seed flow rate, inlet silane flow rate and system temperature. The model results are compared with analytical and experimental results in Fig. 20 where S is seed flow rate, D_{ap} is average particle diameter, D_{as} is average seed particle diameter and Y is silicon production rate.

Parker [105] simulated silane deposition in FBR based on an experimental reactor operated at the Jet Propulsion Laboratory (JPL) [86,88,87,89]. A kinetic model similar to that followed by Balaji et al. above was adopted, namely consisting of two routes: the heterogeneous decomposition of silane onto Si particles (following simple Arrhenius type kinetics) and the homogeneous decomposition of silane into fines which are then scavenged by Si particles. The scavenging reaction rate is given by the following expression:

$$r_{scav} = \frac{d(\rho_{fines})}{dt} (M_{Si})^{-1} = -\alpha \frac{S_{Si}}{V_R} \frac{\rho_{fines}}{M_{Si}} \quad (20)$$

where α is a scavenging constant, and $\frac{S_{Si}}{V_R}$ is surface area of silicon particles per reactor volume.

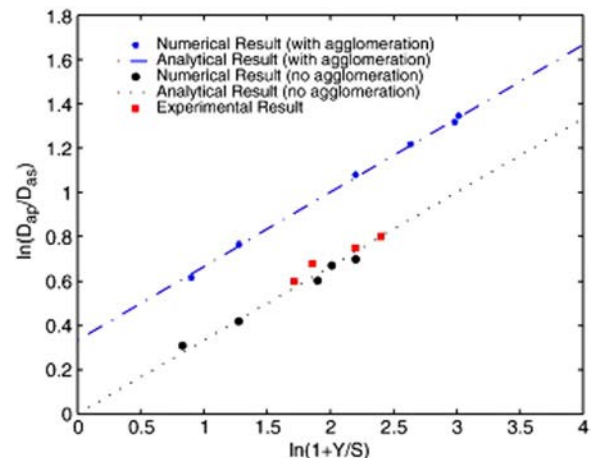


Fig. 20. Comparison of numerical and analytical model results with experimental results for Balaji's multi-scale model [103]. S is seed flow rate, D_{ap} is average particle diameter, D_{as} is average seed particle diameter and Y is silicon production rate.

Multi-phase CFD calculations were carried out using the Barracuda software package utilizing the Computational Particle Fluid Dynamics (CPFD[®]) numerical method [106–108], which can handle a wide range of particle loading in the same simulation domain. Two types of inlets were tested, a uniform screen distributor (producing bubbling bed) and a nozzle (producing spouting bed). Gas flow was ramped up from zero over 5 s, a uniform particle size distribution was assumed with a constant particle volume fraction and isothermal conditions at 923 K. The inlet screen results closely matched experimental results for deposition of silicon and fines production in reactor, both of which increased with increased silane feed to the reactor. Overall the screen input produced greater silicon deposition (with greater difference from nozzle input with increasing silane feed fraction) while the nozzle input produced substantially greater silicon fines. It was found that for the nozzle input, a large percentage of the silane is transported right through the bed without getting the chance to deposit and instead forms fines in the space above them.

Reuge and Caussat [110] investigated the mechanism of sub-micrometer size agglomerate formation during CVD. They used two models, the first of which assumed stable particles modeled using analytical equations of diffusion/reaction were used for chemical vapor infiltration in porous media. The second approach was for dynamically particles (permanently renewed) and used MFIX. They found that gaseous diffusion into the agglomerates was not a limiting step, that high deposition rates mainly occur within a small zone within a few millimeters of the silane entrance point and are the main cause of agglomeration formation in this region and that lower deposition rates can be achieved by temperatures as low as 723 K.

Du et al. [111] sought to develop a model to predict silicon yield as a function of operating conditions. This involved integrating a two phase reaction module (incorporating bubble and emulsion phases), a particle growth module (based on PBM) and a fluid dynamics module implemented in COMSOL. Du and Ydstie [112] had previously developed a similar particle growth model using discrete population balance. The fluid dynamics module predicts velocity and bed density as solid volume fraction, feeds these profiles into the reaction module and particle growth modules and the latter's results are fed back into the fluid dynamic module. The authors validated the model with experimental results and used it to develop a multivariable control scheme.

Liu and Xiao [113] used a coupled Eulerian-granular (CFD-PBM) model to study 3-D FBR. The general modeling strategy for this model is shown in Fig. 21. The three node quadrature method of moments (QMOM) CFD-PBM model was developed by them in an earlier work [114] in which it was found that particle growth occurs mainly by scavenging. The kinetics were modeled in two main parts; gas phase

species transport and silane decomposition using a homogeneous kinetic model based on global kinetic models of Hogness et al. [109] and Furusawa et al. [83] while silane deposition on particle surface was represented using heterogeneous kinetic models of Iya et al. [82] and Furusawa et al. [83]. The authors sought to validate their model using the experimental results of Hsu et al. [86] and recreated the latter's FBR geometry for their simulations. Simulation results are shown in Fig. 22 and overall agreed well with Hsu's experiments. Overall it was found that surface deposition rate decreased as one moves up the bed and increases with higher silane mole fraction (especially above 0.2).

4.5. Miscellaneous reactor designs

Early modeling studies on a horizontal single wafer reactor with suspended substrate for silicon epitaxial film deposition were carried out by Habuka et al. [70], with experimental validation. They used momentum, heat and mass transport equations solved in 2-D using FLUENT and chemical reactions taking place by Eley-Rideal mechanism at the substrate surface. They found that the governing processes were chemisorption of TCS and its decomposition by hydrogen. This was followed up by a study [119] in which they investigated the same system but with 3-D transport and epitaxy model. They largely confirmed experimental data by finding a nonlinear increase of epitaxial deposition with increasing TCS concentration at the reactor inlet with the major mechanism of such an increase being mainly due to changes in rate of surface processes mainly caused by changed in surface coverage.

Pera et al. [120] analyzed a reactor for fast inline CVD of silicon from silane for producing silicon ribbons as part of a Silicon over Dust Substrate (SDS) process. This involved moving a substrate along the reactor and radiative heat sources with elliptical mirrors placed along the reactor to create narrow uniform lines of radiation perpendicular to displacement direction. Gas entered and exited the reactor in turbulent regimes and hydrogen was used to model all gases. CFD found that the heating zones create convection flows strongly dependent on reactor geometry. When the distance between heating zones was double the height of the chamber, cylindrical shape convection flows were obtained, two for each heating zone and were said to increase deposition rates. For a ratio less than 0.5, the cylinders distorted in length and eventually became rectangular flow regimes. Changing reactor walls to adiabatic from aluminum reduced flow variation along reactor width and produced a regime parallel to the length which promoted homogeneity deposition.

A horizontal rib reactor was looked at for TCS CVD by Zhang et al. [121]. Their model was based on the horizontal flat reactor of Habuka et al. [70], with a rib added to the upper wall, and simulated 2-D steady state flow. FLUENT was used to solve the flow equations, including mass diffusion in turbulent flows, with discretization accomplished using SIMPLE. Mass transport was balanced by substrate reaction, with the deposition reaction being a boundary condition of species transport. The Eddy-Dissipation-Concept (EDC) model was used to model turbulence-chemistry interactions. Kinetics were based on the reaction mechanism of Valente et al. [122]. The rib reactor lead to an average rate of deposition 1.9 times that of the flat reactor. The rib lead to a thinner boundary layer near the center of the reactor and a higher temperature gradient. The rib also increased heat flux to the substrate but decreased heat flux uniformity. Zhang et al. [123] then followed up with a study investigating boundary layer effects in a flat horizontal reactor, a rib reactor and a reactor with tilted substrate. They found that the momentum boundary layer significantly affects the thermal boundary layer, which in term impacts the deposition rate. In terms of species concentration, they found that TCS concentration at the substrate should remain high while HCl should be decreased after deposition to avoid reduced deposition rates.

Wei et al. [124] simulated a horizontal reactor with turbulent flow using Reynolds Averaged Navier-Stokes (RANS) equations and studied

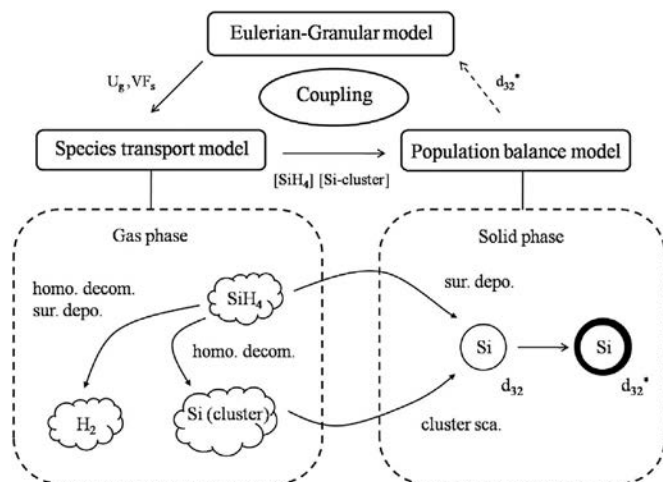


Fig. 21. The general modeling strategy of the coupled Eulerian-Granular or CFD-PBM model used by Liu and Xiao [113].

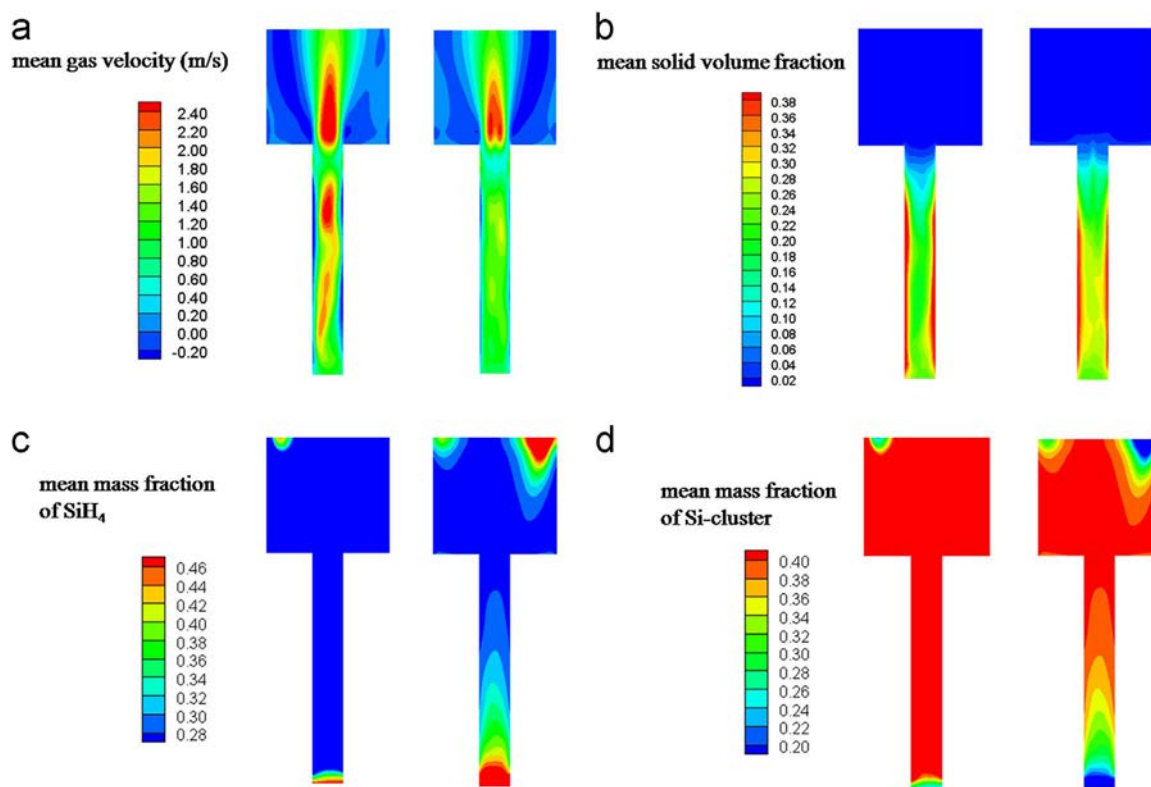


Fig. 22. Simulation result visualizations of the coupled CFD-PBM model of Liu and Xiao used with homogeneous kinetics to model the FBR used in experiments by Hsu et al. [86], displaying (a) mean gas velocity, (b) mean solid volume fraction, (c) mean mass fraction of silane and (d) mean mass fraction of Si-cluster. For each result (a–d), the left heat map represents kinetics based on the work of Hogeness et al. [109] while the right represents kinetics of Furusawa et al. [83].

the effects of Rayleigh and Reynolds (Re) number on Si deposition. They found that, contrary to industry expectation, turbulent CVD can provide uniform heat transfer and Si deposition when time averaged. They also found it possible to achieve quite high deposition rates due to better reactant mixing but requires careful control to avoid transversal non-uniform deposition with too high Re numbers.

Masi et al. [125] simulated a flame assisted chemical vapor deposition (FACVD) reactor for silicon thin film production. This type of reactor consists of a cold wall chamber with a susceptor that holds the substrate and a hydrogen-halogen flame burner in the center which generates heat and pushes precursors (also routed into the chamber at the center next to the burner) to the substrate. They used three models in conjunction, starting from simplest to more complex; a 2D axial symmetric model, a 1D simplified plug flow reactor model and zero-dimensional continuously stirred tank reactor (CSTR) model. Both silane and TCS based deposition kinetics were used. Silane was found to produce greater deposition and precursor usage for the same conditions as opposed to TCS. Running at near atmospheric conditions, FACVD was found to use 40% less energy than traditional plasma or rapid thermal CVD while also cutting costs. Another exotic reactor design was studied looked at by Rehmet et al. [126], where they conducted numerical modeling of nanocrystalline silicon deposition by STC hydrogenation in radio-frequency (RF) plasma reactors.

4.6. Thermal phenomena and heat loss

The uneven temperature profile of electrically heated polysilicon rods was studied by Del Coso et al. [127]. They modeled a cylindrical rod with arbitrary radius, surrounded by a cylindrical reflective wall with a mixture of TCS and H_2 flowing around the rod. The model was symmetric except along the length of the rod (z), with current density flowing only in the z -direction due to a time-harmonic electrical current. Heat was generated by the Joule effect and produced radial

dependent temperature and conductivity distribution. The silicon was assumed to behave as intrinsic at high temperatures, while Maxwell's equations inside a semiconductor were used to produce the Helmholtz equation for an electric field. Calculations were conducted for steady state and took into account heat flow within the rod, convection and the deposition chemical reaction (simplified to a single equation from two steps). The system of equations was solved using non-linear methods and the finite difference method. Generally the center of the rod was at hotter temperature then the surface due to higher current flow in that region. Increasing frequency of the current pushed it to outer regions due to the skin effect and decreased the temperature difference between the center and outer regions. Thus, the rod temperature profile could be made more uniform, reducing thermal stresses and allowing increased rod diameters. Increasing wall reflectivity also increased temperature uniformity while a higher convection coefficient had the opposite effect.

The radiative energy loss in a Siemens bell jar reactor was examined by Del Coso et al. [128]. The radiation exchange between polysilicon rods and the reactor wall was considered with the following assumptions: all surfaces are considered diffuse and gray which allows reflected and emitted energies to be combined into a single energy flux leaving the surface, the silicon rods are assumed to be infinitely long which allowed calculation of configuration factors following Hottel's crossed-string method and the reactor wall and rods (1373 K) are at fixed temperatures. The reactor contained 36 polysilicon rods arranged with radial symmetry. Two cases were considered, one consisting of rods and reactor wall only and another consisting of rods, reactor wall and thermal shields. For the first case analytical expressions for the irradiance, directly emitted energy flux and radiosity were utilized to conduct an energy balance and derive an expression for net radiation heat exchanged by each surface. Thermal shields were cylinders surrounding the rods and had unknown temperature, but still assumed to only transfer heat by radiation. An

energy balance was first conducted for a single heat shield followed by a balance for all shields which assumed under steady state conditions the same heat passes through all the shields and they are infinitely long cylinders.

Overall, rods towards the center of the reactor radiated less power to the wall than those in outer rings, with the difference increasing substantially with increasing rod diameter. There was also significant decrease in power radiated to the wall with the addition of thermal shields, however the shields reached very high temperatures which would likely result in polysilicon deposition on them. Increasing the number of rods decreased the average power emitted per rod to the reactor wall while increasing average silicon growth rate also decreased energy radiation. Decreasing wall emissivity through material selection was also another source of energy savings.

Huang et al. [67] carried out a radiative heat loss study, using an adapted S2S radiation model, of the novel Siemens bell jar reactor they developed [66] and which is discussed in Section 4.1. Similar investigations of conventional Siemens reactors, they found that increasing number of rods, reducing inner shield emissivity, increasing inner shield temperature and increasing polysilicon growth rate can reduce energy loss.

Ramos et al. [129] also investigated radiative heat loss from polysilicon rods in a bell jar reactor. They carried out a similar energy balance to obtain net heat flux exchanged for a certain surface area. Their calculations were validated through comparison with a reactor for single and four rod configurations and subtracting convective heat loss and chemical reaction enthalpies from total power consumption to obtain radiation heat loss. A 36 rod industrial scale reactor was then numerically modeled while varying various parameters. Radiation heat loss per rod increased with increasing wall emissivity, increasing wall radius (slight effect), decreasing rod diameter and increasing rod surface temperature. This was followed up with a study on the same system utilizing the radiation heat loss model with additions of heat loss through gas conduction and convection effects [130]. The convective heat loss was based on the analytical solution for a cylinder in parallel flow with consideration of both natural and forced convection. The obtained model was validated through experiments. It was found that radiation was the main form of heat loss followed by conduction and then convection.

Nie et al. [131] studied the effect enlarging reactor capacity (in terms of number of rods) on heat loss in a Siemens bell jar type reactor. They used a discrete ordinates radiation model with expressions for surface irradiance and reflected energy flux based Del Coso's work [128]. They found that increasing capacity, and hence number of rods, leads to lower radiative heat loss as does decreasing wall emissivity. In a separate study, Nie et al. [132] developed a model for electric heating by DC current in a 24 rod Siemens reactor. Heat transfer by convection and radiation were modeled using k - ϵ model in ANSYS FLUENT and thermal and electrical behavior of the rods was modeled by the Joule effect in COMSOL. They validated their model with industrial data and found that results for outer rods showed greater error than for inner rods, although both had relative error within 10%. It was found that the temperature gradient was higher for rods in the outer ring and that increasing rod radius towards the end of the deposition process would reduce energy consumption.

Theoretical models of heat loss and thermal distribution in a Siemens bell reactor and a FBR were developed by Ramos et al. [133]. CFD models were represented by axi-symmetric models with global model accounting developed using SiSim software [134–136]. For the 3D systems, the dependent variables were velocities, pressure, temperature and radiosity. Time dependent variables were solved through incompressible Navier-Stokes equations consisting of the continuity equation, energy conservation equation and surface-to-surface radiation model. The surface-to-surface radiation model [137] made use of view factors calculated using the hemicube method [138].

The bell reactor model contained a single silicon rod and was

divided into four domains: the rod, the casing (stainless steel), the fluid flow domain (hydrogen and TCS) and cooling (water to control wall temperature). Three different rod temperatures were simulated and showed a general temperature distribution pattern as seen in Fig. 23. Gas recirculation zones could be observed, caused by the sudden contraction and expansion of the chamber. There was good agreement between model results and laboratory scale experimental results. Increasing wall emissivity and flow rate both decreased rod, wall and outlet temperatures.

The FBR model consisted of a cylindrical chamber divided into the following domains: baseplate (aluminum, synthetic wool and stainless steel), casing (stainless steel), fluid flow (hydrogen and silane), heaters (induction coil), wall isolation (ceramic foam) and cooling (water). No silicon particles were included in the model to avoid dealing with particle dynamics and their energy consumption was distributed to the reactor solids. Two cases, corresponding to high and low inlet flow rates, were simulated. Differences between experiments (which involved a reactor also containing silicon beads) and simulation were below 5% for most parameters. However, for the low inlet flow case, the baseplate and lower region temperature (T_{gas1}) differed significantly from experiment with underestimation of values by the model. This occurred because the axi-symmetrical model deviates from the real baseplate geometry. On the other hand, for the high inlet flow case, the wall temperatures differed significantly with overestimation of values by the model. This was likely due to lack of silicon bead simulation which causes difference in gas velocity and heat transfer coefficient. Varying the gas composition, reactor wall emissivity and heat transfer coefficients between interfaces had little impact on temperature distribution. Increasing the flow rate generally decreased temperature, with greater effect further from the baseplate. Lowering the baseplate thermal conductivity increased temperatures near this region only.

5. First principles atomistic modeling

There have been a number of ab initio studies focused mainly on gas phase reactions of the various chemical species (consisting of Si, Cl, C and H atoms) present throughout the different stages of the Siemens process. Almost all of these studies used quantum chemistry methods involving Møller-Plesset (MP) perturbation theory and transition state theory (or canonical variational transition state theory for reactions without a transition state) usually implemented through the Gaussian-n theory composite methods. Unless specifically mentioned, the following studies can be assumed to follow these methods. Su et al. studied thermal decomposition of monosilanes such as TCS and STC and obtained rate constants [139]. Swihart and Carr continued the same thermal decomposition study with chlorinated disilanes [140] and followed up by looking at the thermal decomposition of TCS, DCS and SiH_3Cl in hydrogen [141]. Several similar studies dealing with various decomposition reactions of silanes and chlorosilanes or their reactions with Cl, H or H_2 were also conducted in the 2000 s period [142–149].

Although these investigations were not specifically for silicon hydrochlorination, often focusing on Si CVD or even SiC CVD [148,149], the results can be applied to both processes as they contain the same species with just direction of reactions sometimes differing. While most of these papers were not comprehensive studies combining all of the possible reactions in the reacting system with reaction rate constants obtained from mechanistic studies of elementary reactions, the piecemeal Si CVD system studies could be used as starting points for such a model. An early effort by Swihart and Carr [141] mentioned above used 39 elementary reactions among 20 species. In a recent such work incorporating the largest number of reactions so far, Ran et al. [150] employed the G3B3 method to study kinetics parameters for 117 reactions involving 20 species. However, Kuniishi et al. [38] in their plug flow reactor study mentioned in Section 3.1.4 chose not to use this model as it ignored Si_2 species, instead choosing to use the 26 reaction

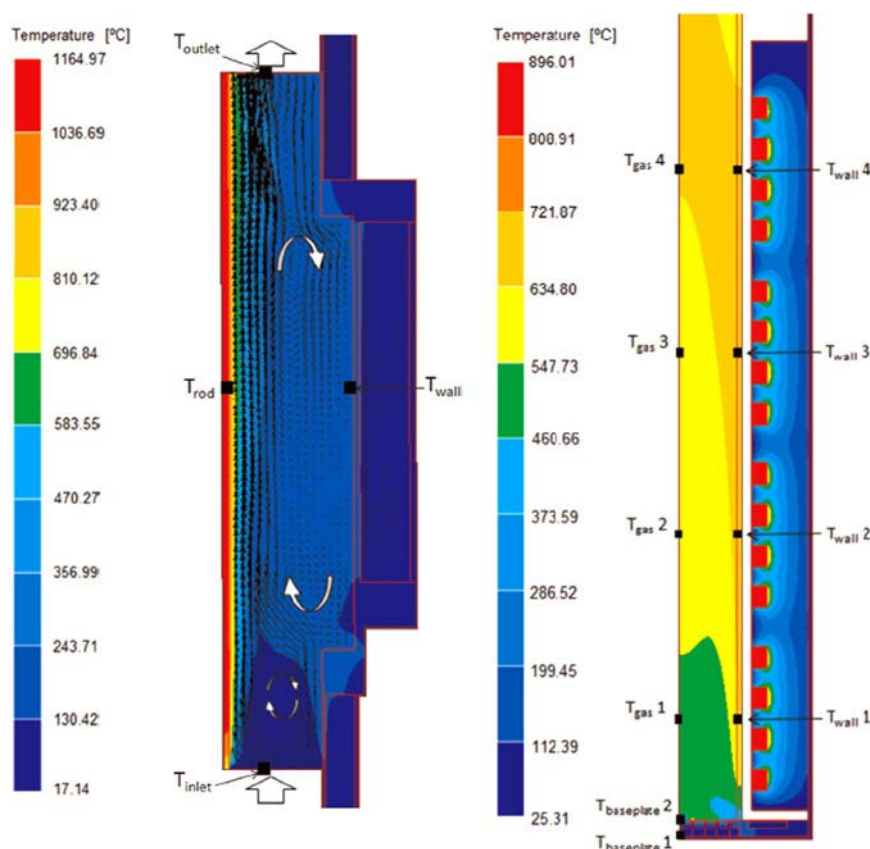


Fig. 23. Thermal distribution modeling of solid and gas phases done by Ramos et al. [133] for silicon deposition reactors while excluding reactions. Temperature distribution and fluid flow field (black arrows) for bell jar reactor with TCS and hydrogen gases (on left) and temperature distribution for fluidized bed reactor with silane and hydrogen gases (on right).

and 16 species model of Ravasio et al. [50] as a starting basis. Data from the previously mentioned ab initio studies were then added in addition to several more [151–153]. Dkhissi et al. [154] compared DFT and composite quantum chemistry methods for compounds in a Si-Zn system where Zn is used to reduce STC directly to Si(s). They found that the BMK functional for DFT and CBS-QB3 composite method were most suited for the silicon production process, especially those also containing transition state metals such as Zn. Kuniyoshi et al. [155] looked at Si surface reactions with H₂ and HCl for cluster size effects.

Pandey et al. [156] looked at plasma deposition of amorphous silicon thin films from silane. They looked at surface conditions where silyl (SiH₃) was the dominant deposition precursor using kinetic Monte Carlo simulations (accounting for surface reaction and diffusion processes). The early stages of growth at low surface coverage were simulated using a database of activation barriers determined by DFT calculations with the processes identified by molecular dynamics. Later stage growth, which approached steady state at monolayer coverage, accounted for interaction effects between adsorbed species by using binding energy variance calculated through DFT. The results predicted surface silyl concentration dependence with temperature, surface H content and dangling-bond coverage. Such a model may be adapted to conventional Siemens derived processes.

6. Current challenges and future research directions

The previous sections demonstrate that the stage corresponding to synthesis of intermediate Si based compounds (primarily through hydrochlorination of MG-Si) has had relatively fewer studies when compared to the Si deposition step. The former stage has been modeled primarily as simple 1-D systems, with only Wang [35] attempting 2-D models, often using analytical relationships for processes such as particle size change and particle fluidization. Furthermore, all of these

attempts make a number of simplifying assumptions such as steady state conditions, ideal gases, uniform densities of gas and particles and laminar flow. Hence, there is a need for completely 3-D models incorporating fully developed turbulent fluid flow coupled with reaction kinetics as formulated for several Si deposition stage FBR studies. This will also aid in exploring reactor configurations and shapes which may improve performance as was done by Huang et al. [66] for a bell jar reactor. A possible design option for fixed bed reactors would be looking at a preheat stage which can be run at optimal temperatures for gas phase reactions while allowing the solid-gas reactions in the bed region to be run at a different optimized temperature.

The use of FBRs for TCS decomposition as replacement of bell jar reactors has received very little attention, especially when compared to the extensive literature present on FBRs for silane pyrolysis. The high temperatures required for TCS decomposition also contribute towards problematic deposition of silicon reactor walls and heating surfaces. This combined with the corrosive gas mixtures present has decreased enthusiasm for experimental investigation of such FBRs. However, these challenges are well suited for study through theoretical modeling techniques which can freely explore many reactor configurations and operating conditions without costly and difficult experiments. They also aid in the development of novel designs such as the nozzle injection and internally circulating designs outlined in Section 4.2. However, even those two studies did not consider any reactions in the system and only looked at fluid flow or hydrodynamic behavior of particles. Clearly, there is a need for models of FBR reactor designs for TCS decomposition that simulate 3D multiphase reacting systems as well as exploration of other novel designs which can overcome the technical challenges.

A particular challenge common to many studies is the empirical or semi-empirical fitting of certain parameters which causes the model to be not reliable outside of certain operating parameters. Here there is a

role for first principles based atomistic studies which could potentially provide parameters such as activation energies as inputs for higher scale models. This has been attempted by Kunioishi et al [38] in their inquiry into STC hydrogenation in which they used previous ab initio studies' literature to obtain kinetic parameters. However, this models only part of the process taking part in MG-Si hydrochlorination and needs to be applied in other studies involving more comprehensive reaction systems, especially with regards to the various Si deposition stage studies which assume very simple reaction kinetics and use old empirical values.

Furthermore, multiple catalysts (in addition to the CuCl_2 for Si hydrochlorination analyzed by Ding et al. [32]) should be explored for each reacting stage of the polysilicon process. There is a need for a better understanding of surface effects and catalytic behavior, for which atomistic studies are also well suited. Although there has been some preliminary work done using cluster systems [155], more thorough investigations using accurate techniques and taking into account long range crystal structure, the multiple species and reactions present in these systems and free energy considerations is needed. Specifically the quantum chemistry techniques used in the ab initio studies to date are not the most suitable for large models involving solid surfaces and other techniques such as density functional theory with the latest accurate functionals should be tried. Ultimately, these earlier models should build towards multi-scale models incorporating comprehensive reaction systems (Balaji et al. [103] do adopt a multi-scale approach but their reaction system could incorporate more complexity and does not use micro or nano-scale techniques).

7. Conclusion

This work provided a review of studies involving chemical and physical modeling of solar grade silicon production, with a specific focus on the Siemens process and its derivatives and silane pyrolysis. An overview of various methods for solar grade silicon refining and the stages of the Siemens process was first conducted. This was followed by sections on two major stages of the Siemens process and its modifications. The first section, on the synthesis of volatile Si based compounds from MG-Si, looked at hydrochlorination of MG-Si (with subsections discussing fixed bed reactors, fluidized bed reactors, thermodynamic equilibria and catalysts) and production of silane through reactive distillation. The second section looked at the deposition of these volatile Si based compounds to form SOG-Si with subsections discussing TCS deposition in bell jar reactors, silane pyrolysis in bell jar reactors, silane pyrolysis in fluidized bed reactors, miscellaneous novel reactor designs and thermal and heat loss phenomena. A brief review of ab initio atomistic modeling with regards to SOG-Si refining was also presented. Finally, there was a discussion of the shortcomings of current theoretical models for these processes and future directions which should be explored. The information available in this review should supply good starting points for those looking to choose models to utilize in studying parts of the SOG-Si refining process or looking to expand on earlier work in constructing their own model.

Acknowledgements

The authors would like to thank Natural Sciences and Engineering Research Council of Canada (NSERC), Mitacs, Ubiquity Solar Inc., and the University of Toronto in providing funding support for this work.

References

- [1] Andrews Ross Needham, Claron Stephen John. Pathways to Solar Grade Silicon. *Silicon* 2015;7(3):303–5.
- [2] Global pv demand outlook 2015–2020: Exploring risk in downstream solar markets. gtmresearch, GreenTech Media; 2015.
- [3] Global market outlook for solar power 2015–2019. SolarPower Europe, 2015.
- [4] Mohit Anand. Global pv manufacturing attractiveness index 2015 (pvmax).

- gtmresearch, GreenTech Media; 2015.
- [5] Pandey AK, Tyagi VV, Selvaraj Jeyraj A/L, Rahim NA, Tyagi SK. Recent advances in solar photovoltaic systems for emerging trends and advanced applications. *Renew Sustain Energy Rev* 2016;53:859–84.
- [6] Photovoltaics report. Fraunhofer Institute for Solar Energy Systems; 2016.
- [7] Tyagi VV, Rahim Nurul AA, Rahim NA, Selvaraj Jeyraj A/L. Progress in solar PV technology: research and achievement. *Renew Sustain Energy Rev* 2013;20(443–461).
- [8] Parida Bhubaneswari, Iniyar S, Goic Ranko. A review of solar photovoltaic technologies. *Renew Sustain Energy Rev* 2011;15(3):1625–36.
- [9] Fu Ran, James Ted L, Woodhouse Michael. Economic measurements of polysilicon for the photovoltaic industry: market competition and manufacturing competitiveness. *IEEE J Photovolt* 2015;5(2):515–24.
- [10] Ranjan S, Balaji S, Panella Rocco a, Erik Ydstie B. Silicon solar cell production. *Comput Chem Eng* 2011;35(8):1439–53.
- [11] Bye Gøran, Ceccaroli Bruno. Solar grade silicon: technology status and industrial trends. *Sol Energy Mater Sol Cells* 2014;130:634–46.
- [12] Yasuda Kouji, Morita Kazuki, Okabe Toru H. Processes for production of solar-grade silicon using hydrogen reduction and/or thermal decomposition. *Energy Technol* 2014;2(2):141–54.
- [13] Lynch David, Ben Wade, Ji Xiaoyang, Jiang Feng, Salce Alex, Morey Evan, Jiao Yubo. *Rev Dev Prod Silicon Photovolt* 2011;1:685–92.
- [14] Spenke E, Heywang W. Twenty five years of semiconductor-grade silicon. *Phys Status Solidi (a)* 1981;64(1):11–44.
- [15] Moriyama Joichiro. Production of high-purity silicon. *Rev iv Suiyokwai-Shi* 1989;21(52).
- [16] Sugiura M, Fuwa A. Kinetic-study of silicon precipitation from SiHCl_3 . *J Jpn Inst Metals* 1994;58(4):436–41.
- [17] Zhai Pei, Williams Eric D. Dynamic hybrid life cycle assessment of energy and carbon of multicrystalline silicon photovoltaic systems. *Environ Sci Technol* 2010;44(20):7950–5, [pmid:20860380].
- [18] Ivanov VM, Trubitsin YuV. Approaches to hydrogenation of silicon tetrachloride in polysilicon manufacture. *Russ Microelectron* 2011;40(8):559–61.
- [19] Yaws Carl L, Jelen Fred C, Li Ku-Yen, Patel PM, Fang CS. New technologies for solar energy silicon: cost analysis of ucc silane process. *Sol Energy* 1979;22(6):547–53.
- [20] Filtvedt WO, Javidi M, Holt A, Melaen MC, Marstein E, Tathgar H, Ramachandran PA. Development of fluidized bed reactors for silicon production. *Sol Energy Mater Sol Cells* 2010;94(12):1980–95.
- [21] LI Jianlong, CHEN Guanghui, ZHANG Pan, WANG Weiwen, DUAN Jihai. Technical Challenges and Progress in Fluidized Bed Chemical Vapor Deposition of Polysilicon. *Chin J Chem Eng* 2011;19(Oct. 5):747–53.
- [22] Filtvedt WO, Holt a, Ramachandran Pa, Melaen MC. Chemical vapor deposition of silicon from silane: review of growth mechanisms and modeling/scaleup of fluidized bed reactors. *Sol Energy Mater Sol Cells* 2012;107:188–200.
- [23] Yanqing Hou, Zhifeng Nie, Gang Xie, Rongxing Li, Xiaohua Yu, Ramachandran Plant A. Thermodynamic behaviors of SiCl_2 in silicon deposition by gas phase zinc reduction of silicon tetrachloride. *Chin J Chem Eng* 2015;23(3):552–8.
- [24] Ceccaroli B, Ovrelid E, Pizzini S. *Solar silicon processes: technologies, challenges, and opportunities*. CRC Press; 2016.
- [25] Karabanov Sergey, Yasevich Victor, Suvorov Dmitriy, Slivkin Evgeniy, and Karabanov Andrey. *Mediterranean Green Buildings & Renewable Energy*. Springer International Publishing, Cham, 2017.
- [26] Karabanov SM, Yasevich VI, Suvorov DV, and Karabanov AS. Mathematical modeling and experimental research of the method of plasma chemical purification of metallurgical-grade silicon. In: 2016 IEEE Proceedings of the 16th International Conference on Environment and Electrical Engineering (EEEIC), pages 1–5, June 2016.
- [27] Safarian J, Tangstad M. Vacuum refining of molten silicon. *Metall Mater Trans B* 2012;43(6):1427–45.
- [28] Yasuda Kouji, Nohira Toshiyuki, Kobayashi Katsutoshi, Kani Naoya, Tsuda Tetsuya, Hagiwara Rika. Improving purity and process volume during direct electrolytic reduction of solid SiO_2 in molten CaCl_2 for the production of solar-grade silicon. *Energy Technol* 2013;1(4):245–52.
- [29] Sugiura Masahito, Kurita Kurita, Nisida Takuo, and Fuwa Akio. Hydrogenation Reactions and Their Kinetics for $\text{SiCl}_4(\text{g})\text{-H}_2(\text{g})$ and $\text{SiCl}_4(\text{g})\text{-Si}(\text{s})\text{-H}_2(\text{g})$ Systems Using a Fixed Bed Type Reactor. *Materials Transactions, JIM*, 33(12):1138–1148, 1992.
- [30] Seo ESM, Brocchi EA, Carvalho RJ, Soares EP, Andreoli M. A mathematical model for silicon chlorination. *J Mater Process Technol* 2003;141(nov 3):370–8.
- [31] Kato K, Kubota H, Wen CY. Mass transfer in fixed and fluidised beds-fluidization fundamentals and application. *Chem Eng Progress* 1970;66(105):87–99.
- [32] Ding Wei-jie, Wang Zhi-bo, Yan Jian-min, Xiao Wen-de. CuCl -Catalyzed hydrogenation of silicon tetrachloride in the presence of silicon: mechanism and kinetic modeling. *Ind Eng Chem Res* 2014;53(43):16725–35.
- [33] Noda Suguru, Tanabe Katsuaki, Yahiro Takashi, Osawa Toshio, Komiyama Hiroshi. Reaction of Si with HCl to Form Chlorosilanes. *J Electrochem Soc* 2004;151(6):C399.
- [34] Jain MP, Sathiyamoorthy D, Govardhana Rao V. Studies on hydrochlorination of silicon in a fixed bed reactor. *Indian Chem Eng* 2010;51(4):272–80.
- [35] Wang Xin. Two-Dimensional Temperature Distribution in Fluidized Bed Reactors for Synthesizing Trichlorosilane. Thesis, Submitted. The Hong Kong University of Science and Technology; 2011.
- [36] Ding Wei-Jie, Yan Jian-Min, Xiao Wen-De. Hydrogenation of silicon tetrachloride in the presence of silicon: thermodynamic and experimental investigation. *Ind Eng Chem Res* 2014;53(27):10943–53.

- [37] Wu Jijun, Chen Zhengjie, Ma Wenhui, Dai Yongnian. Thermodynamic estimation of silicon tetrachloride to trichlorosilane by a low temperature hydrogenation technique. *Silicon* 2015;0–6. [pages].
- [38] Kunioishi Nilson, Moriyama Yu, and Fuwa Akio. Kinetics of the Conversion of Silicon Tetrachloride into Trichlorosilane Obtained through the Temperature Control along a Plug-Flow Reactor. *International Journal of Chemical Kinetics*, p. n/a-n/a; 2015.
- [39] Colomb Matthias, Palanki Srinivas, Sylvester Nicholas D. Modeling the hydrochlorination reaction in a laboratory-scale fluidized bed reactor. *Powder Technol* 2016;292(may):242–50.
- [40] Daizo Kunii, Levenspiel Octave. Bubbling bed model. model for flow of gas through a fluidized bed. *Ind Eng Chem Fundam* 1968;7(3):446–52.
- [41] Kato K, Wen CY. Bubble assemblage model for fluidized bed catalytic reactors. *Chem Eng Sci* 1969;24(8):1351–69.
- [42] Daizo Kunii, Levenspiel Octave. Fluidized reactor models. 1. for bubbling beds of fine, intermediate, and large particles. 2. for the lean phase: freeboard and fast fluidization. *Ind Eng Chem Res* 1990;29(7):1226–34.
- [43] Chitester Douglas C, Kornosky Robert M, Fan Liang-Shih, Danko Joseph P. Characteristics of fluidization at high pressure. *Chem Eng Sci* 1984;39(2):253–61.
- [44] Wen CY, Yu YH. A generalized method for predicting the minimum fluidization velocity. *AIChE J* 1966;12(3):610–2.
- [45] Becker Frank. Modellierungen und Simulationen der Hydrochlorierung von Silizium zu Trichlorosilan für die Entwicklung eines technischen Wirbelschichtreaktors. [Ph.D. thesis], Aachen; 2005.
- [46] Geldart D. Types of gas fluidization. *Powder Technol* 1973;7(5):285–92.
- [47] Yasui George, Johanson LN. Characteristics of gas pockets in fluidized beds. *AIChE J* 1958;4(4):445–52.
- [48] Werther Joachim. Scale-up modeling for fluidized bed reactors. *Chem Eng Sci* 1992;47(9):2457–62.
- [49] Zhao Muyu, Wang Zichen, Xiao Liangzhi. Determining the number of independent components by brinkley's method. *J Chem Educ* 1992;69(7):539.
- [50] Ravasio Stefano, Masi Maurizio, and Cavallotti Carlo. Analysis of the gas phase reactivity of chlorosilanes. *The Journal of Physical Chemistry A*, 117(25):5221–5231, 2013. pmid:23731215.
- [51] Huang Xun, Ding Wei-Jie, Yan Jian-Min, Xiao Wen-De. Reactive distillation column for disproportionation of trichlorosilane to silane: reducing refrigeration load with intermediate condensers. *Ind Eng Chem Res* 2013;52(may 18):6211–20.
- [52] Shuaishuai Sun, Guoqiang Huang. Simulation of reactive distillation process for monosilane production via redistribution of trichlorosilane. *Chin J Chem Eng* 2014;22(3):287–93.
- [53] Rafael Alcántara - Avila J, Delgado Hugo Alberto Sillas, Segovia - Hernández Juan Gabriel, Gómez - Castro Fernando I, Cervantes - Jauregui Jorge A. Silane production through reactive distillation with intermediate condensers, 37. Elsevier; 2015 <http://www.sciencedirect.com/science/article/pii/B9780444635778500188>.
- [54] Alcántara-Avila JRafael, Hasebe Shinji, Kano Manabu. New synthesis procedure to find the optimal distillation sequence with internal and external heat integrations. *Ind Eng Chem Res* 2013;52(13):4851–62.
- [55] Zang Xinxiang, Huang Kejin, Yuan Yang, Chen Haisheng, Zhang Liang, Wang Shaofeng, Wang Kun. Reactive distillation columns with multiple reactive sections: a case study on the disproportionation of trichlorosilane to silane. *Ind Eng Chem Res* 2017;56(jan 3):717–27.
- [56] Li Xue-Gang, Huang Xun, Xiao Wen-De. Reactive distillation-aided ultrapur silane production from trichlorosilane: process simulation and optimization. *Ind Eng Chem Res* 2017;56(7):1731–8.
- [57] Ulrich Gael D, Vasudevan Palligamai T. How to estimate utility costs. *Chem Eng* 2006;113(4):66.
- [58] Nie Zhi Feng, Xie Gang, Hou Yan Qing, Cui Yan, Li Rong Xing, Yu Zhan Lian. Fluid dynamic simulations on polysilicon production. *Appl Mech Mater* 2013;444–445:991–5.
- [59] Ni Haoyin, Lu Shijie, Chen Caixia. Modeling and simulation of silicon epitaxial growth in Siemens CVD reactor. *J Cryst Growth* 2014;404(89–99).
- [60] Magnussen Bjørn F. The eddy dissipation concept - a bridge between science and technology. ECCOMAS thematic conference on computational combustion.
- [61] Mathur SR, Murthy JY. Coupled ordinates method for multigrid acceleration of radiation calculations. *J Thermophys Heat Transf* 1999;13(4):467–73.
- [62] Balakrishna Ajit, Chacin Juan M, Comita PB, Haas B, Ho P, Thilderkvist A. Chemical kinetics for modeling silicon epitaxy from chlorosilanes. In: Proceedings of the 194th Meeting of the Electrochemical Society, US DOE, MA, pages 1-6, 1998.
- [63] Ni Hao Yin, Chen Cai Xia. Computational Results Show Gas Phase Reactions Have Great Impact on the Deposition Rate of Silicon in Siemens CVD Reactors. *Advanced Materials Research*, 1104:39–44; 2015.
- [64] Caretto LS, Gosman AD, Patankar SV, Spalding DB. Two calculation procedures for steady, three-dimensional flows with recirculation. In: Proceedings of the third international conference on numerical methods in fluid mechanics, pages 60–68. Springer; 1973.
- [65] Pope SB. Computationally efficient implementation of combustion chemistry using in situ adaptive tabulation. *Combust Theory Model* 1997;1(1):41–63.
- [66] Huang Z, Liu C, Yuan X, Liu S, Liu F. Development of a Polysilicon Chemical Vapor Deposition Reactor Using the Computational Fluid Dynamics Method. *ECS J Solid State Sci Technol* 2013;2(sep 11):P457–P464.
- [67] Huang Zhe Qing, Ding Hao, Wang Xiaojing, Liu Chun Jiang. Numerical Solution for Radiative Heat Transfer in a Novel Polysilicon CVD Reactor. *Numer Heat Transf* 2013;64(9):744–58.
- [68] del Coso G, del Cañizo C, Luque a. Chemical vapor deposition model of polysilicon in a trichlorosilane and hydrogen system. *J Electrochem Soc* 2008;155(6):D485.
- [69] Huang Zheqing, Qie Siyuan, Quan Xiaoyu, Guo Kai, Liu Chunjiang. Numerical simulation of multiple polysilicon CVD reactors connected in series using CFD method. *Can J Chem Eng* 2015;93(10):1721–9.
- [70] Habuka Hitoshi, Nagoya Takatoshi, Mayusumi Masanori, Katayama Masatake, Shimada Manabu, Okuyama Kikuo. Model on transport phenomena and epitaxial growth of silicon thin film in SiHCl₃-H₂ system under atmospheric pressure. *J Cryst Growth* 1996;169(1):61–72.
- [71] Carlo Cavallotti, Maurizio Masi. Kinetics of SiHCl₃ chemical vapor deposition and fluid dynamic simulations. *J Nanosci Nanotech* 2011;11(9).
- [72] Odden Jan Ove, Halvorsen Gunnar, Rong Harry, Glöckner Ronny. Comparison of the energy consumption in different production processes for solar grade silicon. *Silicon Chem Sol Ind IX*, Oslo, Nor 2008:75–90.
- [73] Moon Hokyu, Kim Hwang Suk, Song Jiwoon, Lee Hwanseong, Kwon Hyun Goo, Jung Yoon sub, Cho Hyung Hee. Effect of extended single/multi-jet nozzles in a fluidized bed reactor on growth of granular polysilicon. *Chem Eng J* 2014;248:242–52.
- [74] Madhava Syamlal, O'Brien Thomas J. Fluid dynamic simulation of O₃ decomposition in a bubbling fluidized bed. *AIChE J* 2003;49(11):2793–801.
- [75] Li Peilong, Yu Xinyu, Liu Fang, Wang Tiefeng. Hydrodynamic behaviors of an internally circulating fluidized bed with wide-size-distribution particles for preparing polysilicon granules. *Powder Technol* 2015;281:112–20.
- [76] Gidaspow Dimitri. Multiphase flow and fluidization: continuum and kinetic theory descriptions. Academic press, 1994.
- [77] Jung Hosub, Park Jong Hoon, Kang Seung Oh, Jeong Jong Hyun, Jeon Soyung, Jung Jae Hak, Kim Woo Kyoung. Computational Fluid Dynamics Modeling of Mono-Silane Siemens Reactor. *Japanese Journal of Applied Physics*, 51:10NA10; 2012.
- [78] Jeon Soyung, Jung Hosub, Park Jong Hoon, Kim Woo Kyoung. Effect of rod diameters on flow pattern and temperature profile in monosilane siemens Poly-Si reactor. *Mol Cryst Liq Cryst* 2013;585(1):73–81.
- [79] Kang Seung Oh, Lee Uk June, Kim Seung Hyun, You Ho Jung, Park Kun, Park Sung Eun, Park Jong Hoon. Gas nozzle effect on the deposition of polysilicon by monosilane siemens reactor. *Int J Photo* 2012(2012):1–6.
- [80] Gang Li Xue, De Xiao Wen. Silane pyrolysis to silicon rod in a bell-jar reactor at high temperature and pressure: Modeling and simulation. *Indus Eng Chem Res* 2016;55(17):4887–96.
- [81] Hashimoto Kenji, Miura Kouichi, Masuda Takao, Toma Masaaki, Sawai Hiroyuki, Kawase Motoaki. Growth kinetics of polycrystalline silicon from silane by thermal chemical vapor deposition method. *J Electrochem Soc* 1990;137(3):1000–7.
- [82] Iya SK, Flagella RN, DiPaolo FS. Heterogeneous decomposition of silane in a fixed bed reactor. *J Electrochem Soc* 1982;129(7):1531–5.
- [83] Furusawa Takehiko, Kojima Toshinori, Hiroha Hiroyuki. Chemical vapor deposition and homogeneous nucleation in monosilane pyrolysis within interparticle spaces - application of fines formation analysis to fluidized bed CVD-. *Chem Eng Sci* 1988;43(8):2037–42.
- [84] Praturi Ananda K, Lutwack R, Hsu G. Chemical vapor deposition of silicon from silane pyrolysis; 1977.
- [85] Lai S, Dudukovic' MP, Ramachandran PA. Chemical vapor deposition and homogeneous nucleation in fluidized bed reactors: silicon from silane. *Chem Eng Sci* 1986;41(4):633–41.
- [86] Hsu G, Hogle R, Rohatgi N, Morrison A. Fines in fluidized bed silane pyrolysis. *J Electrochem Soc* 1984;131(3):660–3.
- [87] Naresh K. Rohatgi. Silicon production in a fluidized bed reactor: final report. Pasadena, CA (USA): Technical report, Jet Propulsion Lab; 1986.
- [88] Hsu G. Fluidized-bed development at jpl. In *Flat-Plate Solar Array Project Workshop on Low-Cost Polysilicon for Terrestrial Photovoltaic Solar-Cell Applications*, vol. 1, p. 147–65; 1986.
- [89] Hsu George, Rohatgi Naresh, Houseman John. Silicon particle growth in a fluidized-bed reactor. *AIChE J* 1987;33(5):784–91.
- [90] Guenther C, Incorporated Fluent, Brien TO, and Syamlal M. A numerical model of silane pyrolysis in a gas-solids fluidized bed. *International Conference on Multiphase Flow*, pages 1–12; 2001.
- [91] Xie Nan, Francine Battaglia, and Rodney O Fox. Simulations of multiphase reactive flows in fluidized beds using in situ adaptive tabulation. *Combust Theory Model* 2004;8(2):195–209.
- [92] Fayolle Francine. Analyse et modélisation des dépôts d'oxyde de silicium par procédé LPCVD. [Ph.D. thesis], Toulouse, INPT; 1993.
- [93] Cadoret L, Reuge N, Pannala S, Syamlal M, Coufort C, Caussat B. Silicon CVD on powders in fluidized bed: experimental and multifluid Eulerian modelling study. *Surf Coat Technol* 2007;201:8919–23, [22-23 SPEC. ISS].
- [94] Schaeffer David G. Instability in the evolution equations describing incompressible granular flow. *J Differ Equ* 1987;66(1):19–50.
- [95] Reuge N, Cadoret L, Caussat B. Multifluid eulerian modelling of a silicon fluidized bed chemical vapor deposition process: analysis of various kinetic models. *Chem Eng J* 2009;148(2–3):506–16.
- [96] Srivastava A, Sundaresan S. Analysis of a frictional-kinetic model for gas-particle flow. *Powder Technol* 2003;129(1–3):72–85.
- [97] Howell John R. Thermal radiation heat transferr and robert siegel. Hemisphere Publishing Corporation; 1992.
- [98] Coltrin Michael E, Kee Robert J, Miller James A. A mathematical model of silicon chemical vapor deposition: further refinements and the effects of thermal diffusion. *J Electrochem Soc* 1986;133(6):1206–13.
- [99] Coltrin Michael E, Kee Robert J, Evans Greg H. A mathematical model of the fluid mechanics and gasphase chemistry in a rotating disk chemical vapor deposition

- reactor. *J Electrochem Soc* 1989;136(3):819–29.
- [100] Kleijn CR. Computational modeling of transport phenomena and detailed chemistry in chemical vapor deposition - a benchmark solution. *Thin Solid Films* 2000;365(2):294–306, [cited by 62].
- [101] Buss Richard J, Ho Pauline, Breiland William G, Coltrin Michael E. Reactive sticking coefficients for silane and disilane on polycrystalline silicon. *J Appl Phys* 1988;63(8).
- [102] Breiland William G, Coltrin Michael E. Si deposition rates in a twodimensional cvd reactor and comparisons with model calculations. *J Electrochem Soc* 1990;137(7):2313–9.
- [103] Balaji S, Du Juan, White CM, Erik Ydstie B. Multi-scale modeling and control of fluidized beds for the production of solar grade silicon. *Powder Technol* 2010;199(1):23–31.
- [104] White Christy M, Ege Paul, and Ydstie B. Erik. Size distribution modeling for fluidized bed solar-grade silicon production. *Powder Technology*, 163(1-2):51-58, 2006. Fluidization and Fluid Particle Systems Papers chosen by the {AIChE} Area 3b Committee on Fluidization and Fluid Particle Systems, drawn from a selection of papers presented at the 2004 {AIChE} Annual Meeting held in Austin, 7-12 November 2004.
- [105] Parker James M. Validation of CFD Model for Polysilicon Deposition and Production of Silicon Fines in a Silane Deposition FBR. *Int J Chem React Eng* 2011;9(1).
- [106] Snider DM. An incompressible three-dimensional multiphase particle-in-cell model for dense particle flows. *J Comput Phys* 2001;170(June 2):523–49.
- [107] Snider Dale M. Three fundamental granular flow experiments and {CPFD} predictions. *Powder Technol* 2007;176(1):36–46.
- [108] O'Rourke Peter J, Zhao Paul (Pinghua), Snider Dale. A model for collisional exchange in gas/liquid/solid fluidized beds. *Chem Eng Sci* 2009;64(8):1784–97.
- [109] Hogness TR, Wilson Thomas L, Johnson Warren C. The thermal decomposition of silane. *J Am Chem Soc* 1936;58(1):108–12.
- [110] Reuge Nicolas, Caussat Brigitte. Modeling of silicon CVD into agglomerates of Sub-micrometer-size particles in a fluidized bed. *Chem Vap Depos* 2011;17(10–12):305–11.
- [111] Du Juan, Dutta Soham, Ydstie Birger Erik. Modeling and control of solar-grade silicon production in a fluidized bed reactor. *AIChE J* 2014;60(5):1740–51.
- [112] Du Juan, Ydstie BE. Modeling and control of particulate processes and application to poly-silicon production. *Chem Eng Sci* 2012;67(1):120–30.
- [113] Liu Si-Si, Xiao Wen-De. CFD-PBM coupled simulation of silicon CVD growth in a fluidized bed reactor: effect of silane pyrolysis kinetic models. *Chem Eng Sci* 2015;127:84–94.
- [114] Liu Si-Si, Xiao Wen-De. Numerical simulations of particle growth in a silicon-cvd fluidized bed reactor via a cfd-pbm coupled model. *Chem Eng Sci* 2014;111:112–25.
- [115] Syamlal Madhava. Mfix documentation numerical technique; 1998.
- [116] Spalding DB. Numerical computation of multi-phase uid ow and heat transfer, p. 139–67; 1980.
- [117] Patankar SV. Numerical Heat Transfer and Fluid Flow. Hemisphere Publishing Corporation: Electro Skills Series; 1980.
- [118] White CM, Zeininger G, Ege P, Ydstie BE. Multi-scale modeling and constrained sensitivity analysis of particulate cvd systems. *Chem Vap Depos* 2007;13(9):507–12.
- [119] Habuka Hitoshi, Katayama Masatake, Shimada Manabu, Okuyama Kikuo. Nonlinear increase in silicon epitaxial growth rate in a sihcl3h2 system under atmospheric pressure. *J Cryst Growth* 1997;182(3):352–62.
- [120] Pera D, Augusto A, Alves J Maia, Brito MC, Serra JM, and Valléra AM. Inline fast CVD ssystem for continuous production of silicon ribbons for solar cells by the SDS process. Conference Record of the IEEE Photovoltaic Specialists Conference, pages 000210-000213; 2009.
- [121] Zhang Pan, Wang Wei Wen, Wu Yu Lei, Chen Guang Hui, Li Jian Long. CFD Study on Polycrystalline Silicon Chemical Vapor Deposition in a Rib Reactor. In 2010 Asia-Pacific Power and Energy Engineering Conference, number 4, pages 1-4. IEEE; 2010.
- [122] Valente Gianluca, Cavallotti Carlo, Masi Maurizio, Carr Sergio. Reduced order model for the {CVD} of epitaxial silicon from silane and chlorosilanes. *Journal of Crystal Growth*, 230(1–2):247-257, 2001. In: Proceedings of the Third International Workshop on Modeling in Crystal Growth.
- [123] Zhang Pan, Wang Weiwen, Cheng Guanghui, Li Jianlong. Effect of boundary layers on polycrystalline silicon chemical vapor deposition in a trichlorosilane and hydrogen system. *Chin J Chem Eng* 2011;19(1):1–9.
- [124] Wei Jiaying, Xu Rui, Yu Yanfei, Hou Jinliang, Li Changfeng. Simulation and analysis of Si deposition in turbulent CVD reactors. *J Semicond* 2014;35(8):083002.
- [125] Masi M, Cavallotti C, Raffa E. Modeling of flame assisted chemical vapor deposition of silicon films. *Cryst Res Technol* 2011;46(8):865–70.
- [126] Rehmet Christophe, Cao Tengfei, Cheng Yi. Numerical study of Si nanoparticle formation by SiCl 4 hydrogenation in RF plasma. *Plasma Sources Sci Technol* 2016;25(2):025011.
- [127] del Coso G, Tobias I, Canizo C, Luque A. Temperature homogeneity of polysilicon rods in a Siemens reactor. *J Cryst Growth* 2007;299(1):165–70.
- [128] Coso Gonzalo Del, Canizo Carlos del, Luque Antonio. Radiative energy loss in a polysilicon CVD reactor. *Sol Energy Mater Sol Cells* 2011;95(4):1042–9.
- [129] Ramos A, Del Cañizo C, Valdehita J, Zamorano JC, Luque A. Radiation heat savings in polysilicon production: validation of results through a CVD laboratory prototype. *J Cryst Growth* 2013;374:5–10.
- [130] Ramos a, Rodríguez a, del Cañizo C, Valdehita J, Zamorano JC, Luque a. Heat losses in a CVD reactor for polysilicon production: comprehensive model and experimental validation. *J Cryst Growth* 2014;402:138–46.
- [131] Nie Zhi Feng, Xie Gang, Hou Yan Qing, Cui Yan, Yu Zhan Liang, Tian Lin. Numerical simulation of polysilicon chemical vapor deposition in siemens reactor. *Mater Sci Forum* 2015;833(107–111).
- [132] Nie Zhifeng, Hou Yanqing, Xie Gang, Cui Yan, Yu Xiaohua. Electric heating of the silicon rods in Siemens reactor. *Int J Heat Mass Transf* 2015;90:1026–33.
- [133] Ramos A, Filtvedt WO, Lindholm D, Ramachandran PA, Rodríguez A, del Cañizo C. Deposition reactors for solar grade silicon: a comparative thermal analysis of a Siemens reactor and a fluidized bed reactor. *J Cryst Growth* 2015;431:1–9.
- [134] Bellmann MP, Lindholm D, Srheim EA, Mortensen D, M'Hamdi M. 3d dynamic simulation of heat transfer and melt flow in an inductively heated crystallization furnace for mc-silicon with {PID} temperature control. *J Cryst Growth* 2013;383:119–25.
- [135] Mortensen Dag, Lindholm Dag, Friestad Kenneth, Henriksen Bjrn Rune, Fjr Hallvard G, Rudshaug Magne, Srheim Einar A. Crystallization furnace modeling including coupled heat and fluid flow, stresses and deformations. *Energy Procedia* 2013;38:597–603.
- [136] Bellmann MP, Lindholm D, M'Hamdi M. A novel method for gas flow and impurity control in directional solidification of multi-crystalline silicon. *J Cryst Growth* 2014;399:33–8.
- [137] Modest Michael F. Radiative heat transfer. Academic Press; 2013.
- [138] Cohen Michael F, Greenberg Donald P. The hemi-cube: a radiosity solution for complex environments. *SIGGRAPH Comput Graph* 1985;19(3):31–40.
- [139] Su Ming Der, Schlegel Bernard H. An ab initio MO study of the thermal decomposition of chlorinated monosilanes, SiH₄-nCl_n (n=0–4). *J Phys Chem* 1993;97(39):9981–5.
- [140] Swihart Mark T, Carr Robert W. Thermochemistry and thermal decomposition of the chlorinated disilanes (Si₂ > H n Cl 6- n, n=0–6) Studied by ab Initio molecular orbital methods. *J Phys Chem A* 1997;101(40):7434–45.
- [141] Swihart MT, Carr RW. On the mechanism of homogeneous decomposition of the chlorinated silanes. Chain React propagated divalent Silicon Species *J Phys Chem A* 1993;102(9):1542–9.
- [142] Wittbrodt Joanne M, Schlegel Bernhard H. An ab initio study of the thermal decomposition of dichlorosilane. *Chem Phys Lett* 1997;265(3):527–31.
- [143] Zhang Qingzhu, Wang Shaokun, Gu* Yueshu. Direct ab initio dynamics studies of the reactions of h with sih₄-ncl_n (n=1–3). *J Phys Chem A* 2002;106(15):3796–803.
- [144] Pei Kemei, Li Haiyang. Ab initio and kinetic calculations for the reactions of cl with SiHnCl_{4-n}?(n=1,2,3,4). *J Chem Phys* 2004;121(14).
- [145] Zhang Xiang, Ding Yi-hong, Li Ze-sheng, Huang Xu-ri, Sun Chia-chung. Ab initio study on the rate constants of sicl₄ . h [rightward arrow] sicl₃ . hcl. *Phys Chem Chem Phys* 2001;3:965–9.
- [146] Walch Stephen P, Dateo Christopher E. Thermal decomposition pathways and rates for silane, chlorosilane, dichlorosilane, and trichlorosilane. *J Phys Chem A* 2001;105(10):2015–22.
- [147] Walch Stephen P, Dateo Christopher E. Reactions of SiCl₂ and SiHCl with h and cl atoms. *J Phys Chem A* 2002;106(12):2931–4.
- [148] Deng Juanli, Su Kehe, Wang Xin, Zeng Qingfeng, Cheng Laifei, Xu Yongdong, Zhang Litong. Thermodynamics of the gas-phase reactions in chemical vapor deposition of silicon carbide with methyltrichlorosilane precursor. *Theor Chem Acc* 2008;122(1):1–22.
- [149] Ge Yingbin, Gordon Mark S, Battaglia Francine, Fox Rodney O. Theoretical study of the pyrolysis of methyltrichlorosilane in the gas phase. 3. Reaction rate constant calculations. *J Phys Chem A* 2010;114(6):2384–92.
- [150] Ran Yi, Wang Jing-Bo, Yin Yong-Xiang. Theoretical study on the SiH₄-nCl_n (n=0–4) reaction mechanisms for polysilicon production process. *Comput Theor Chem* 2014;1035(may 60–67).
- [151] Junko Takahashi, Takama Momose, Tadama Shida. Thermal rate constants for sih₄ SiH₃ + h and CH₄CH₃+h by canonical variational transition state theory. *Bull Chem Soc Jpn* 1994;67(1):74–85.
- [152] Yu Xin, Li Shen-Min, Li Ze-Sheng, Sun Chia-Chung. Direct ab initio dynamics studies of the reaction paths and rate constants of hydrogen atom with germane and silane. *J Phys Chem A* 2000;104(40):9207–12.
- [153] Matsumoto Keiji, Klippenstein Stephen J, Tonokura Kenichi, Koshi Mitsuo. Channel specific rate constants relevant to the thermal decomposition of disilane. *J Phys Chem A* 2005;109(22):4911–20.
- [154] Dkhissi Ahmed, Reyniers Marie Françoise, Marin Guy B. A theoretical study of standard heat of formation of systems involving in the zinc reduction of silicon tetrachloride. *Theor Chem Acc* 2014;134(1).
- [155] Kunioshi Nilson, Anzai Keisuke, Ushijima Harunobu, Fuwa Akio. Effects of cluster size on calculation of activation energies of silicon surface reactions with H₂ and HCl. *J Cryst Growth* 2015;418:115–9.
- [156] Pandey Sumeet C, Singh Tejinder, Maroudas Dimitrios. Kinetic Monte Carlo simulations of surface growth during plasma deposition of silicon thin films. *J Chem Phys* 2009;131(3):034503.